Macromolecules

pubs.acs.org/Macromolecules Article

Role of the Middle Block on Crystallization-Driven Self-Assembly of ABC Copolymers Containing the Crystalline π-Conjugated Polythiophene End Block

Boyang Shi, Ding Shen, Jingwei Zhang, Xiaoxiao Wu, Chengguang Liu, and Guowei Wang*

Cite This: Macromolecules 2025, 58, 8670−8685 Read Online

ACCESS | Metrics & More | Article Recommendations | Supporting Information

ABSTRACT: Modulation of microstructures of copolymers containing π-conjugated poly(3-hexylthiophene) (P3HT) is important due to the close connection between their structures and optoelectronic properties. Crystallization-driven self-assembly of copolymers containing P3HT in solution leads to the formation of regular nano-objects and facilitates their applications. In this work, we prepared a series of polyisoprene-*b*-polystyrene-*b*-poly(3-hexylthiophene) (PI-*b*-PS-*b*-P3HT) triblock copolymers with relatively fixed degree of polymerization (DP) of PI and P3HT blocks, while varying the DP of middle PS block, via the coupling reaction between monoaldehyde end-functionalized P3HT-H/CHO and living anionic PI-*b*-PS$^-$Li$^+$ species. The self-assembly behavior of triblock copolymers was comprehensively studied by varying the parameters of DP_{PS}, annealing temperatures, and solvents. The cooperative self-assembly between different copolymers was also achieved. As the PS block has a changeable solvation or plasticization ability depending on these parameters, the rearrangement or recrystallization of P3HT and the self-assembly process could be modulated accordingly. A library of nano-objects, including the uniform fibers, as well as the rarely reported spheres, zipper-like fibers, block-like fibers, and bead-like fibers, were captured. This work confirmed that the middle PS block played a prominent role in the modulation function on the self-assembly behavior of PI-*b*-PS-*b*-P3HT triblock copolymers, greatly enriching the microstructures of π-conjugated copolymers.

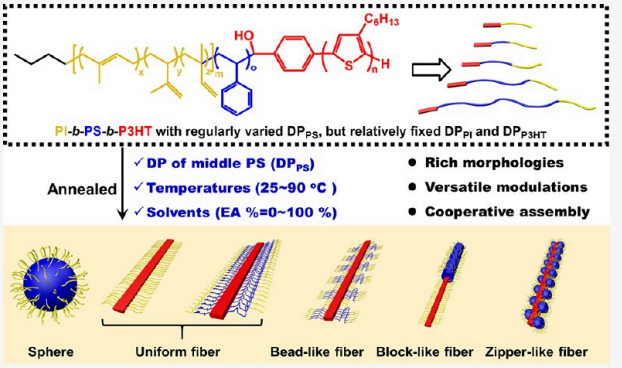

INTRODUCTION

As a π-conjugated polymer, poly(3-hexylthiophene) (P3HT) has been widely studied because of its excellent optical and electronic properties, solution processability, and electrochemical stability for use in organic field-effect transistors (OFETs),[1−3] organic light-emitting diodes (OLED),[4−6] and organic photovoltaics (OPVs).[7−10] However, rapid crystallization of P3HT homopolymers often leads to disordered phases, impairing the charge transport.[11−13] To address this, P3HT is typically incorporated into rod−coil block copolymers in practical applications, and the bulk self-assembly of P3HT-based rod−coil block copolymers has been widely studied. Generally, a flexible coil block in copolymers could promote the crystallization of rod P3HT block and optimize the microstructure for the improved physical and electronic properties.[14−19] For example, Chen et al. prepared a series of P3HT-based diblock copolymers with different coil blocks, including polystyrene (PS), poly(2-vinylpyridine) (P2VP), poly(*n*-butyl acrylate) (P*n*BA), or poly(2-vinylnaphthalene) (PVN).[20] These flexible coil blocks could regulate the morphologies (nanoclusters or nanofibrillars), crystallinities, and charge trapping abilities over a broad range. In particular, the P3HT-*b*-P2VP self-assembled as the nanocluster with an ordered P3HT domain, contributing to high charge transport capability, efficient exciton separation, and fast charge trapping, which could be utilized in a photosynaptic transistor. Similarly, Hong et al. found that the polystyrene-*b*-poly(3-hexylthiophene) (PS-*b*-P3HT) diblock copolymers exhibited up to a 2-fold increase in measured mobility compared to the P3HT homopolymer.[14] Liu et al. prepared the P3HT-*b*-P*n*BA doped with 2,3,5,6-tetrafluoro-7,7,8,8-tetracyanoquinodimethane and developed the stretchable thermoelectric devices with high power factor (PF) and high PF retention, which could not be realized merely utilizing P3HT/P*n*BA homopolymer blends.[21]

Alternatively, the solvent self-assembly provided an improved control over chain ordering for P3HT-based rod−coil block copolymers.[11] Uniquely, the crystallization-driven self-assembly (CDSA) has emerged as an efficient strategy to obtain the well-defined one-dimensional (1D) and two-

Received: May 10, 2025
Revised: July 5, 2025
Accepted: July 29, 2025
Published: August 4, 2025

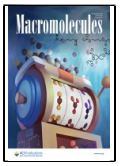

https://doi.org/10.1021/acs.macromol.5c01262
Macromolecules 2025, 58, 8670−8685

Scheme 1. Synthesis and Self-Assembly of PI-*b*-PS-*b*-P3HT Triblock Copolymers

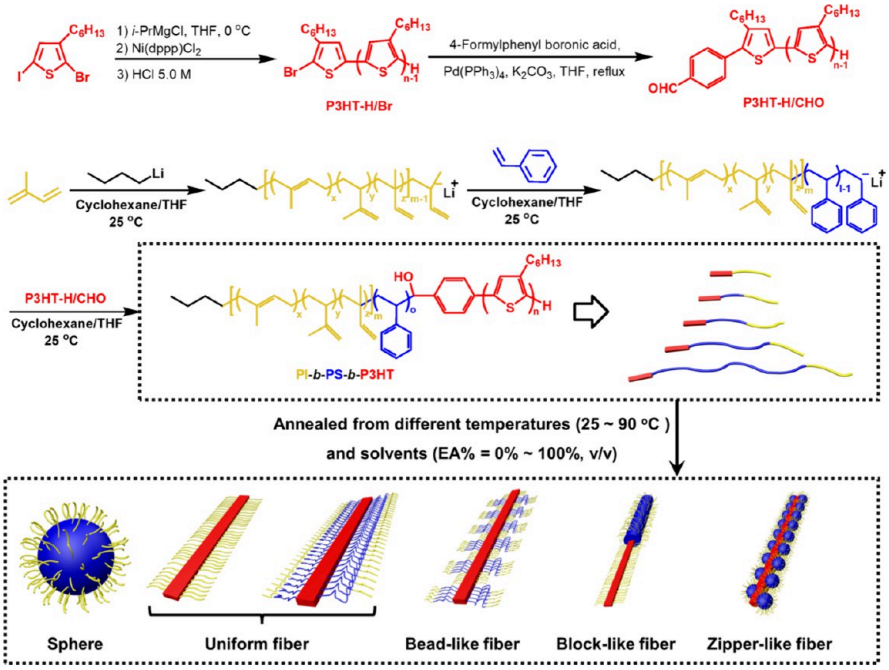

dimensional (2D) nano-objects from block copolymers containing (semi)crystalline blocks.[22−24] Correspondingly, due to the high crystallinity of P3HT block, the block copolymers containing P3HT prefer to self-assemble via the CDSA process,[25,26] which was pioneered by Manners et al. Using poly(3-hexylthiophene)-*b*-poly(dimethylsiloxane) (P3HT-*b*-PDMS) as an example,[27] the long fibers with crystalline P3HT core were successfully prepared via the CDSA process including both self-seeding and seeded growth approaches.[28−32] Similarly, Thelakkat et al. prepared spherical nano-objects via the self-assembly of poly(3-hexylthiophene)-*b*-poly(ethylene glycol) (P3HT-*b*-PEG) in methanol.[33] Qi et al. fabricated 2D rectangular platelets via hierarchical self-assembly of P3HT-*b*-PEG in 2-propanol.[34] These nano-objects facilitated the further applications in organic−inorganic hybrid nanocomposites and organic electronic devices.[30,35,36]

However, to date, the mostly studied rod−coil block copolymers containing P3HT were AB type[14,27,30,33,37] or ABA type,[17,18,38] and the morphologies of the generated nano-objects were dominantly limited as fibers. The examples of ABC-type triblock copolymers containing P3HT are rarely reported and limited in several literature.[39−41] For example, Wu et al. prepared ABC triblock copolymers composed of P3HT, poly(triethylene glycol allene)(PTEGA) and poly-(phenyl isocyanide) (PPI) in one-pot using Ni(II) complex as a single catalyst.[41] The hydrophobic P3HT, hydrophilic PTEGA, and helical PPI comprehensively endowed the triblock copolymers with tunable light emissions and responsiveness to multiple external stimuli including solvents, temperatures, and acids. Higashihara et al. prepared ABC polystyrene-*b*-poly(3-hexylthiophene)-*b*-poly(methyl methacrylate) (PS-*b*-P3HT-*b*-PMMA) triblock copolymer with P3HT as the inner chain by a bilateral click reaction.[40] Stefan et al. prepared ABC polyisoprene-*b*-polystyrene-*b*-poly(3-hexylthiophene) (PI-*b*-PS-*b*-P3HT) triblock copolymer by coupling reaction.[39] However, further investigation on the self-assembly and the application was absent in the latter two cases. Following a general rule between properties and structures, the ternary ABC triblock copolymers might endow the self-assembles with richer morphologies and properties than those from the binary AB diblock or ABA triblock copolymers. The third block would act as a versatile parameter to modulate the function of P3HT-based materials.

Based on the above progress on self-assembly of copolymers containing P3HT and their applications, herein, we designed and synthesized a series of ABC triblock copolymers of PI-*b*-PS-*b*-P3HT with a relatively fixed degree of polymerization (DP) of PI (DP_{PI}) and P3HT (DP_{P3HT}) blocks, with different DP of PS (DP_{PS}) block. The self-assembly of PI-*b*-PS-*b*-P3HT triblock copolymers in *n*-heptane at different annealing temperatures (25−90 °C) or different cosolvents (*n*-heptane/ethyl acetate, Hep/EA) at fixed annealing temperature of 90 °C was comprehensively investigated (Scheme 1). Blending different PI-*b*-PS-*b*-P3HT pairwise in mixed cosolvent (Hep/EA) was also targeted to construct the nano-objects. The transmission electron microscopy (TEM), scanning electron microscopy (SEM), and atomic force microscopy (AFM) were employed to monitor the morphological evolution of the formed nano-objects. For the first time, a series of morphologies including the typical uniform fibers, as well as the rarely reported spheres, zipper-like fibers, block-like fibers, and bead-like fibers, were captured. The ultraviolet−visible (UV−vis) spectroscopy, photoluminescence (PL) spectroscopy, and wide-angle X-ray scattering (WAXS) were used to characterize the microstructures of the P3HT block. The modulation function of the middle PS block on self-assembly behavior of triblock copolymers was focused.

RESULTS AND DISCUSSION

Synthesis and Characterization of the PI-*b*-PS-*b*-P3HT Triblock Copolymer. The PI-*b*-PS-*b*-P3HT triblock copolymers were synthesized by a coupling reaction between the monoaldehyde end-functionalized P3HT-H/CHO and living species PI-*b*-$PS^{-}Li^{+}$ (Scheme 1). To investigate the effect of

https://doi.org/10.1021/acs.macromol.5c01262
Macromolecules 2025, 58, 8670−8685

the middle PS block on the self-assembly behavior of triblock copolymers in the following sections, the degrees of polymerization (DP) of the PI block (DP_{PI}) and the P3HT block (DP_{P3HT}) were designed to be around 150 and 30, respectively, while the DP of the PS block (DP_{PS}) was varied between 0 and 350 (Table S1).

The regioregular P3HT was first synthesized via the Grignard metathesis polymerization (GRIM) method.[42−44] The size exclusion chromatography (SEC) curve showed that the monobromide end-functionalized P3HT-H/Br with a molecular weight (MW) of 5600 g/mol and a narrow molecular weight dispersity ($Đ$ = 1.16) was obtained (Figure S1). The DP_{P3HT} derived from SEC analysis was 33, which was in reasonable agreement with a value of 30 calculated from a proton nuclear magnetic resonance (^{1}H NMR) spectrum based on the resonance signals for protons ($-CH_2(CH_2)_4CH_3$) at 2.82 and 2.64 ppm (Figure S2). The matrix-assisted laser desorption/ionization time-of-flight mass spectrometry (MALDI-TOF MS) analysis confirmed that the end-groups of the P3HT were mainly H/Br (Figure S3), which corresponded to the peaks of ($n \times 166.1$)+1.0+80.0. Subsequently, the $P3HT_{30}$-H/Br was modified to $P3HT_{30}$-H/CHO via Suzuki coupling with 4-formylphenylboronic acid. From the SEC curve, an MW of 5600 g/mol and $Đ$ of 1.14 for $P3HT_{30}$-H/CHO were consistent with those for $P3HT_{30}$-H/Br (Figure S1), confirming the absence of side reaction. From the ^{1}H NMR spectrum, the occurrence of a resonance signal at 10.0 ppm confirmed the successful introduction of an aldehyde group ($-CHO$) onto $P3HT_{30}$-H/CHO (Figure S2). Meanwhile, the MALDI-TOF MS analysis revealed that the peaks were almost shifted from ($n \times 166.1$)+1.0+80.0 for P3HT-H/Br to ($n \times 166.1$)+1.0+106.9 for P3HT-H/CHO (Figure S3), which further verified the successful synthesis of the $P3HT_{30}$-H/CHO precursor.

Subsequently, living species PI^-Li^+ and PI-*b*-PS^-Li^+ were synthesized by sequential living anionic polymerization (LAP) of isoprene (Is) and/or styrene (St) monomers. The SEC curves showed that the PI homopolymer and PI-*b*-PS diblock copolymer with controlled MWs and narrow $Đ$s were prepared (Figure S4), indicating that the LAP in both stages was realized in a controlled manner. Finally, the high reactivity of carbanions toward aldehyde groups ensured the high coupling efficiency between PI^-Li^+ or PI-*b*-PS^-Li^+ and P3HT-H/CHO. The product was purified with a mixture of tetrahydrofuran (THF) and methanol via fractional precipitation, and the reference PI-*b*-P3HT diblock copolymer and target PI-*b*-PS-*b*-P3HT triblock copolymer were obtained by removing the excess PI or PI-*b*-PS. As an example, the SEC curves of the purified PI_{160}-*b*-$P3HT_{30}$ and PI_{135}-*b*-PS_{343}-*b*-$P3HT_{30}$ are shown in Figure S4, which were featured with monomodal peaks and narrow $Đ$s. From the ^{1}H NMR spectra for PI_{160}-*b*-$P3HT_{30}$ and PI_{135}-*b*-PS_{343}-*b*-$P3HT_{30}$ (Figure S5), the characteristic resonance signals at 5.70−4.61 ppm for protons ($-CH=CH_2$, $-CH=CH(CH_3)$, $-CH=C(CH_3)-$) on 1,2-addition, 1,4-addition, and 3,4-addition Is unit on PI, at 7.30−6.30 ppm for aromatic protons ($-C_6H_5$) on PS, at 6.99 ppm for thiophene proton (-S(C−)C*H*-), and at 2.81 ppm for protons ($-CH_2(CH_2)_4CH_3$) on P3HT could be clearly discriminated. Meanwhile, the resonance signal at 10.0 ppm for the aldehyde proton ($-CHO$) on P3HT disappeared completely, further confirming the successful coupling reaction. The SEC and ^{1}H NMR results comprehensively provided solid evidence that the PI-*b*-P3HT diblock copolymer and PI-*b*-PS-*b*-P3HT triblock copolymer were successfully synthesized. The detailed information on the copolymers and their precursors is summarized in Table S1.

Furthermore, the UV−vis and PL spectra were used to characterize the copolymers using THF as a solvent. The absorption spectra of P3HT-H/CHO, PI-*b*-P3HT, and PI-*b*-PS-*b*-P3HT in THF showed the consistent maximum absorption wavelength (λ_{max}) at 445 nm (Figure S6). Meanwhile, the PL spectra of copolymers showed the similar largest emission wavelength (λ_{em}) at 570 nm with an excitation wavelength (λ_{ex}) at 445 nm (Figure S7). The UV−vis and PL spectra were all consistent with the reported results in literature,[27] verifying the characteristic regioregular, π-conjugated structure of P3HT chain in either P3HT-H/CHO or PI-*b*-P3HT and PI-*b*-PS-*b*-P3HT copolymers.

Additionally, the thermal properties of P3HT-H/CHO, PI-*b*-P3HT, and PI-*b*-PS-*b*-P3HT were studied by differential scanning calorimetry (DSC) analysis. In the first cooling run (Figure S8a), the $P3HT_{30}$-H/CHO showed a crystallization temperature (T_c) at 181.2 °C, while the T_cs of PI_{160}-*b*-$P3HT_{30}$ and PI_{135}-*b*-PS_{343}-*b*-$P3HT_{30}$ were lowered to 168.8 to 122.6 °C with the decrease of P3HT content in copolymers. Correspondingly, the crystallization enthalpies of $P3HT_{30}$-H/CHO, PI_{160}-*b*-$P3HT_{30}$, and PI_{135}-*b*-PS_{343}-*b*-$P3HT_{30}$ were gradually decreased as −17.1, −8.4, and −1.7 J/g, respectively. In the second heating run (Figure S8b), the melting temperatures (T_ms) of P3HT in $P3HT_{30}$-H/CHO, PI_{160}-*b*-$P3HT_{30}$, and PI_{135}-*b*-PS_{343}-*b*-$P3HT_{30}$ were detected at 207.1, 210.1, and 212.5 °C, respectively. Although with close T_ms, the melting enthalpies were gradually decreased as 13.8, 8.6, and 2.1 J/g, respectively. From Figure S8c,d, the DSC analysis for PI_{167}-*b*-PS_{42}-*b*-$P3HT_{30}$, PI_{150}-*b*-PS_{85}-*b*-$P3HT_{30}$, and PI_{150}-*b*-PS_{165}-*b*-$P3HT_{30}$ showed the similar evolution tendency of T_cs, T_ms, crystallization enthalpies, and melting enthalpies with the increasing of DP_{PS} in triblock copolymers. Besides the discriminated crystallization behavior of the P3HT block from DSC analysis, the glass transition temperatures (T_gs) of PI and PS blocks were also detected in the second heating run (Figure S8b,d). The T_gs of PS block around 100 °C became obvious at relatively higher DP_{PS}, while the T_gs of PI block around 10 °C could be detected only at relatively lower DP_{PS}. The DSC analysis provided solid evidence that the P3HT in copolymers remained as the crystallization characteristic, however, which was significantly affected by DP_{PS}.

Self-Assembly of PI-*b*-PS-*b*-P3HT Triblock Copolymer in *n*-Heptane from Different Annealing Temperatures. To investigate the self-assembly behavior of PI-*b*-PS-*b*-P3HT triblock copolymers, *n*-heptane was employed as a selective solvent because it exhibits good solubility for the PI block and poor solubility for both PS and P3HT blocks. Critically, the solvation behavior of the PS block in *n*-heptane is temperature-dependent, enabling control over the self-assembly process. By fixing the DP_{PI} and DP_{P3HT} while varying the DP_{PS} and annealing temperatures, the self-assembly process was systematically modulated to fabricate the nanostructures. Typically, 0.10 mL of PI-*b*-PS-*b*-P3HT solution (in dichloromethane, DCM) was added into 10.0 mL of *n*-heptane in a 20 mL vial, and a dispersion with a concentration of 0.20 mg/mL was first formed under stirring. Subsequently, the vial was sealed and the dispersion was left standing in oil bath at 25, 50, 70, or 90 °C for 1.0 h, followed by stopping the heating and natural cooling in oil bath (about 1.5 °C/min) to room temperature (25 °C), and further aging at 25 °C for 24.0 h. On the one

https://doi.org/10.1021/acs.macromol.5c01262
Macromolecules 2025, 58, 8670−8685

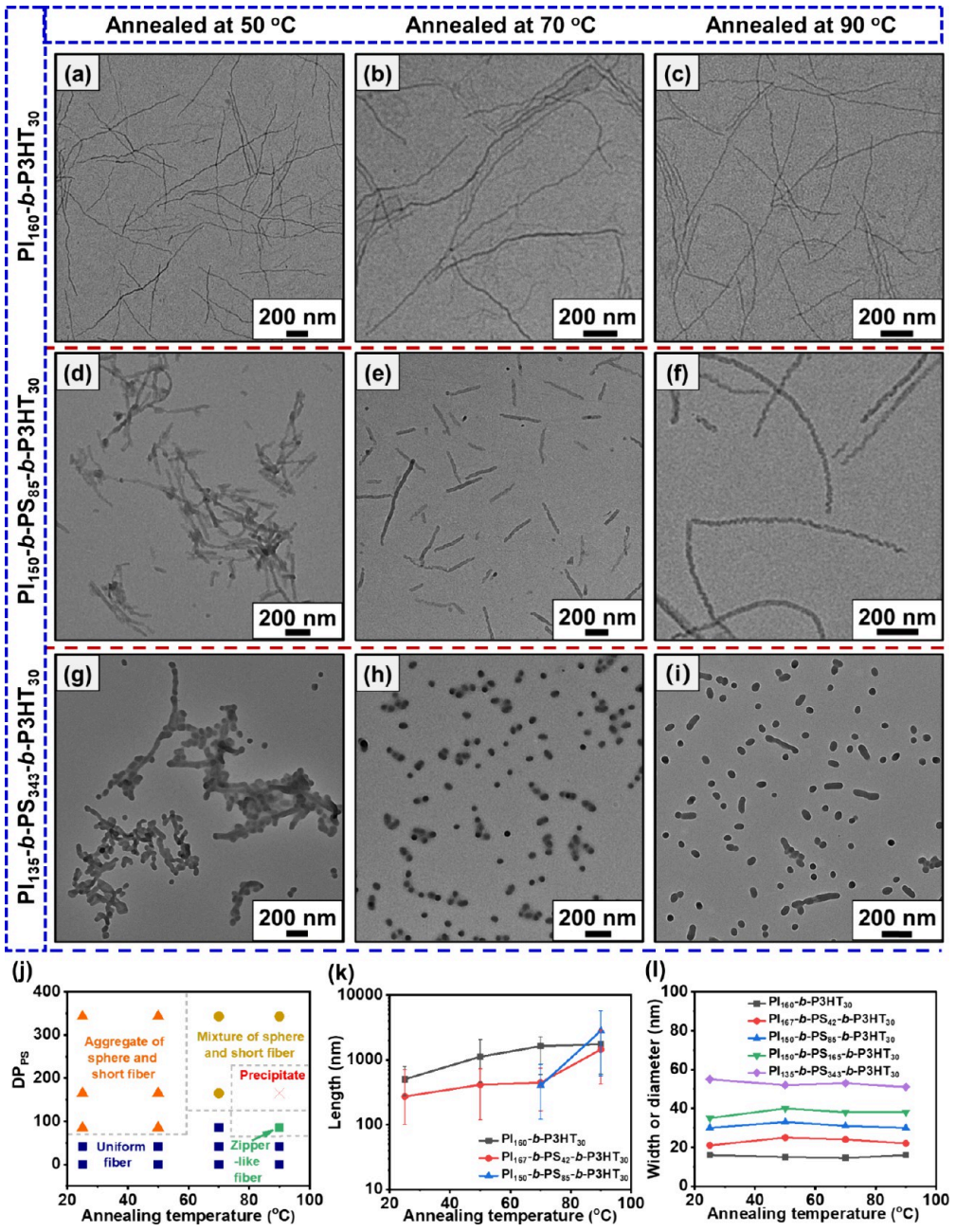

Figure 1. TEM images of nano-objects (diluted into 0.04 mg/mL dispersions) formed by the self-assembly of (a–c) PI_{160}-*b*-$P3HT_{30}$, (d–f) PI_{150}-*b*-PS_{85}-*b*-$P3HT_{30}$, and (g–i) PI_{135}-*b*-PS_{343}-*b*-$P3HT_{30}$ in *n*-heptane annealed at 50, 70, and 90 °C, respectively, and sampled at 25 °C. (j) The morphology diagram of the nano-objects based on the relationship between annealing temperatures and DP_{PS}. (k) Length of fibers vs annealing temperatures. (l) Width of fibers or diameter of spheres vs annealing temperatures.

hand, the DCM was used to accelerate the dissolution or dispersion of PI-*b*-PS-*b*-P3HT triblock copolymers in *n*-heptane. On the other hand, the amount of DCM (1.0% v/v) was relatively low and presumed to have less influence on self-assembly. In all protocols in the following section, the amount of DCM was fixed to the same, and thus, the effect of DCM could be parallelly excluded. Additionally, note that the annealing process was used to remove residual P3HT crystallinity associated with the sample history.

For comparison, the self-assembly of the PI_{160}-*b*-$P3HT_{30}$ diblock copolymer was first monitored. As shown in Figure S9a, after annealing at 25 °C, the PI_{160}-*b*-$P3HT_{30}$ formed fibers with a length of 500 nm and a width of 16 nm. Increasing the annealing temperatures to 50–90 °C, the fiber length was increased to 1.0–2.0 μm with an unchanged width of 16 nm (Figure 1a–c). In this case, the self-assembly yielded fibers with a PI shell and crystalline P3HT core, consistent with a typical CDSA process.[29] Analogous self-assembly behavior was observed for PI_{167}-*b*-PS_{42}-*b*-$P3HT_{30}$, where fiber length scaled with the annealing temperatures: 270 nm from 25 °C, 500 nm from 50 to 70 °C, and over 1.0 μm from 90 °C with an average fiber width of 22 nm (Figures S9b and S10). The identical self-assembly trends between PI_{160}-*b*-$P3HT_{30}$ and PI_{167}-*b*-PS_{42}-*b*-$P3HT_{30}$ demonstrated that a relatively shorter PS block exerted a minimal effect on the self-assembly.

https://doi.org/10.1021/acs.macromol.5c01262
Macromolecules 2025, 58, 8670–8685

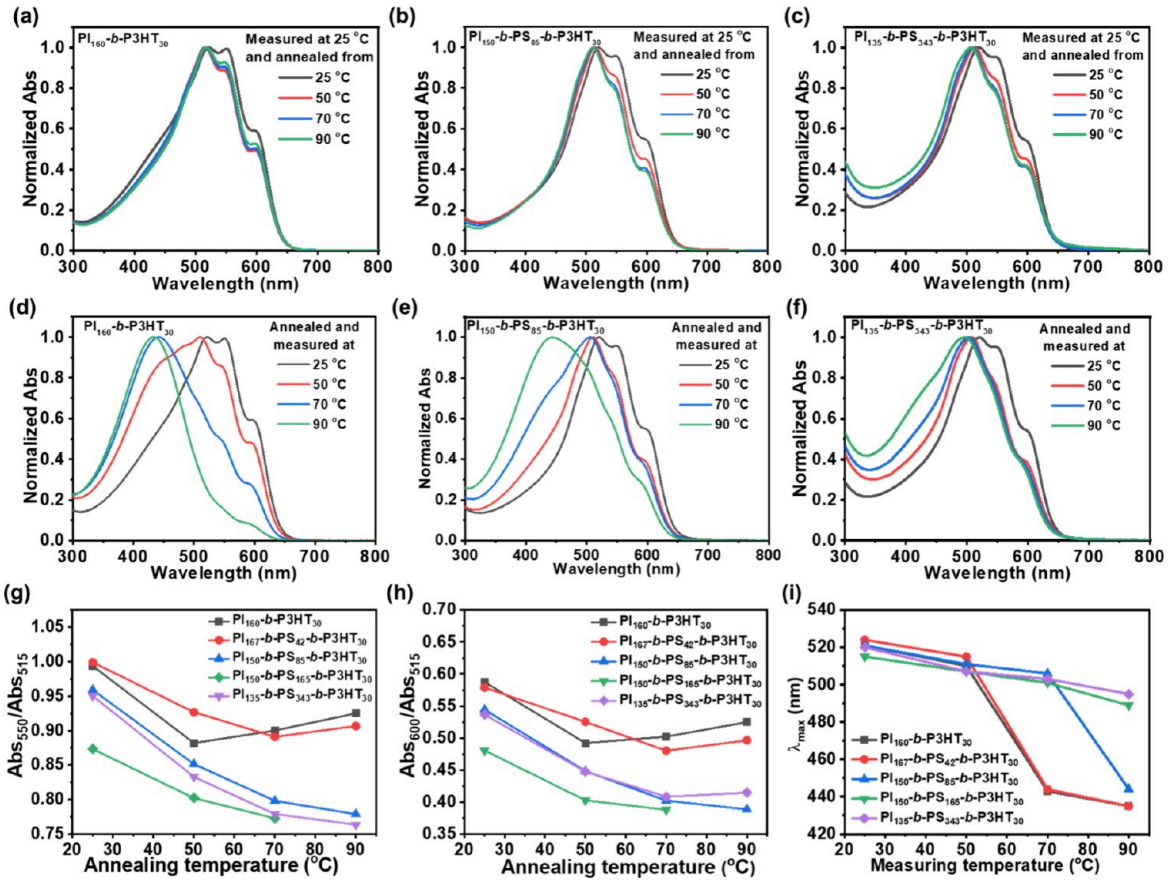

Figure 2. UV−vis spectra for (a) PI_{160}-*b*-$P3HT_{30}$, (b) PI_{150}-*b*-PS_{85}-*b*-$P3HT_{30}$, and (c) PI_{135}-*b*-PS_{343}-*b*-$P3HT_{30}$-based nano-objects in *n*-heptane, annealed at 25, 50, 75, and 90 °C, respectively, and measured at 25 °C. UV−vis spectra for (d) PI_{160}-*b*-$P3HT_{30}$, (e) PI_{150}-*b*-PS_{85}-*b*-$P3HT_{30}$, and (f) PI_{135}-*b*-PS_{343}-*b*-$P3HT_{30}$-based nano-objects in *n*-heptane, annealed and measured at 25, 50, 75, and 90 °C, respectively. The derived curves of (g) Abs_{550}/Abs_{515} and (h) Abs_{600}/Abs_{515} for nano-objects. (i) λ_{max} for PI-*b*-P3HT and PI-*b*-PS-*b*-P3HT based nano-objects annealed and measured at different temperatures.

However, when DP_{PS} was further increased, the self-assembly behavior of PI-*b*-PS-*b*-P3HT changed. For DP_{PS} of 85, the PI_{150}-*b*-PS_{85}-*b*-$P3HT_{30}$ self-assembled as a mixture of spheres and short fibers (length of 180 nm, width of 30 nm) after annealing at 25 and 50 °C (Figure S9c, Figure 1d). When the annealing temperature was increased to 70 °C, the fibers lengthened to about 300 nm, with the width remaining at 30 nm (Figure 1e). Further increasing the annealing temperature to 90 °C, the fibers exceeded 1.5 μm with a persistent width of 30 nm (Figure 1f). Unlike the smooth fibers obtained from PI_{160}-*b*-$P3HT_{30}$, the fibers in Figure 1f had serrated edges with an average pitch of 15 nm, which were labeled as a zipper-like fiber. Consistently, the SEM image further confirmed this unique structure (Figure S11). In the following section, the serrations could be attributed to the solvophobic phase separation of the PS block on the crystalline P3HT core. Continuously, the PI_{150}-PS_{165}-*b*-$P3HT_{30}$ with higher DP_{PS} self-assembled as a mixture of spheres and short fibers (width/diameter of 38 nm) after annealing at 25−70 °C (Figures S9d and S12a,b). However, when the annealing temperature was increased to 90 °C, precipitation occurred during the cooling process. The TEM image of the intermediate (sampled at 45 °C) revealed entangled fibers (Figure S12c). Finally, PI_{135}-*b*-PS_{343}-*b*-$P3HT_{30}$ with the highest DP_{PS} self-assembled as spheres (diameter of 51 nm) under all annealing temperatures, accompanying with trace of short fibers (length of 100−450 nm) (Figure 1g−i, Figure S9e). Notably, in the cases for PI_{150}-PS_{165}-*b*-$P3HT_{30}$ and PI_{135}-*b*-PS_{343}-*b*-$P3HT_{30}$, the higher annealing temperatures (70−90 °C) reduced clustering compared to the lower annealing temperatures (25−50 °C).

Furthermore, the influence of the annealing time on self-assembly was investigated by employing the PI_{150}-*b*-PS_{85}-*b*-$P3HT_{30}$ and PI_{135}-*b*-PS_{343}-*b*-$P3HT_{30}$ as research models and performing the annealing at 90 °C for 20 min, 1.0, and 3.0 h. As shown in Figure S13a−c, under the annealing time of 20 min, 1.0, and 3.0 h, the PI_{150}-*b*-PS_{85}-*b*-$P3HT_{30}$ always formed the zipper-like fibers. Slight difference was that the zipper-like fibers formed at 20 min (about 550 nm length) were shorter than those formed at 1.0 and 3.0 h (over 1.5 μm). It was assumed that, under shorter annealing time, the dissolution and nucleation of PI-*b*-PS-*b*-P3HT triblock copolymers were insufficient and had not reached an equilibrium state, leading to the residual presence of more crystalline seed micelles. Correspondingly, the number of nano-objects increased and shorter zipper-like fibers were collected. As shown in Figure S13d−f, for PI_{135}-*b*-PS_{343}-*b*-$P3HT_{30}$, a mixture of spheres (diameter of 51 nm) and short fibers (length of 100−450 nm) were always formed at 20 min, 1.0, and 3.0 h, and no obvious difference could be discriminated. Thus, these results confirmed that the above annealing time of 1.0 h was sufficient for the dissolution and nucleation of PI-*b*-PS-*b*-P3HT triblock copolymers at 90 °C.

Based on the TEM and SEM images, the morphology diagram correlating annealing temperatures and DP_{PS} was

https://doi.org/10.1021/acs.macromol.5c01262
Macromolecules 2025, 58, 8670−8685

depicted (Figure 1j). In the cases with relatively lower DP_{PS}, the PI-*b*-PS-*b*-P3HT tended to self-assemble as long fibers under all annealing temperatures. Oppositely, with relatively higher DP_{PS}, the aggregate of short fibers and spheres was preferred in the cases at lower annealing temperatures, while a mixture of separated short fibers and spheres were observed at higher annealing temperatures. These results comprehensively illustrated that annealing temperatures and DP_{PS} have a significant effect on the self-assembly process of PI-*b*-PS-*b*-P3HT.

Explanation on the Self-Assembly Mechanism of PI-*b*-PS-*b*-P3HT Triblock Copolymer in *n*-Heptane. To elucidate the modulation mechanism of the middle PS on the self-assembly of PI-*b*-PS-*b*-P3HT and to gain insight into the reason for morphological evolution, the UV−vis spectra of nano-objects were monitored and compared. According to the references,[39,45,46] the red-shifting of λ_{max} from 445 to 515 nm is attributed to the change of $\pi-\pi^*$ transition of P3HT, and the absorption intensities at λ_{550} and λ_{600} corresponded to the interchain $\pi-\pi$ interaction and regular arrangement of the P3HT block. Thus, the λ_{max}, absorption intensity ratios between the shoulder peak and the maximum peak at 550 nm (Abs_{550}/Abs_{515}) and 600 nm (Abs_{600}/Abs_{515}) were derived from the UV−vis spectra and systematically analyzed in the following section.

First, to analyze the microstructure of P3HT block in nano-objects, the UV−vis measurement of nano-objects from different annealing temperatures was performed in *n*-heptane at 25 °C. Compared with the UV−vis spectra of PI-*b*-PS-*b*-P3HT triblock copolymers in THF (Figure S6), all λ_{max} red-shifted from 445 to 515 nm in *n*-heptane (Figure 2a−c, Figure S14). Regularly, the PI_{160}-*b*-$P3HT_{30}$ and PI_{167}-*b*-PS_{42}-*b*-$P3HT_{30}$ nano-objects exhibited higher Abs_{550}/Abs_{515} and Abs_{600}/Abs_{515}, with minima at the annealing temperature of 50 or 70 °C, respectively (Figure 2g,h). The PI_{150}-*b*-PS_{85}-*b*-$P3HT_{30}$, PI_{150}-*b*-PS_{165}-*b*-$P3HT_{30}$, and PI_{135}-*b*-PS_{343}-*b*-$P3HT_{30}$ nano-objects showed relatively lower Abs_{550}/Abs_{515} and Abs_{600}/Abs_{515}, which gradually decreased with the increase of annealing temperatures (Figure 2g,h). Collectively, the UV−vis data reflected that the P3HT block in nano-objects from different PI-*b*-PS-*b*-P3HT triblock copolymers exhibited distinct rearrangement or recrystallization behaviors. For triblock copolymers with lower DP_{PS}, the higher annealing temperature (90 °C) promoted the solvation or dissolution of the P3HT and PS blocks, and the copolymers were readily dissolved as unimers. Without or with less interruption by the PS block, the dissolved unimers could sufficiently rearrange and recrystallize, causing longer fibers with higher crystallinity during the cooling process to 25 °C. Conversely, lower annealing temperatures (25 °C) could not efficiently destroy the original crystalline structure of P3HT block, which was generated by diluting copolymer in DCM with *n*-heptane. Correspondingly, the Abs_{550}/Abs_{515} and Abs_{600}/Abs_{515} for PI_{160}-*b*-$P3HT_{30}$ and PI_{167}-*b*-PS_{42}-*b*-$P3HT_{30}$ showed a valley at 50 or 70 °C, reflecting a balance between the solvation and crystallization of P3HT in *n*-heptane. The result aligned with the classical CDSA theory. For triblock copolymers with higher DP_{PS}, higher annealing temperatures facilitated the formation of unimers. However, the longer PS block would significantly hinder and interrupt the recrystallization of the P3HT block during the cooling process to 25 °C. Therefore, the Abs_{550}/Abs_{515} and Abs_{600}/Abs_{515} for PI_{150}-*b*-PS_{85}-*b*-$P3HT_{30}$, PI_{150}-*b*-PS_{165}-*b*-$P3HT_{30}$, and PI_{135}-*b*-PS_{343}-*b*-$P3HT_{30}$ regularly decreased in a range of 25−90 °C.

Subsequently, to probe the self-assembly dynamics, the UV−vis measurement of nano-objects from different annealing temperatures was also performed in *n*-heptane at the corresponding temperatures. For PI_{160}-*b*-$P3HT_{30}$ and PI_{167}-*b*-PS_{42}-*b*-$P3HT_{30}$ nano-objects, the λ_{max} gradually backed from 515 to 445 nm with the increase of measurement temperatures from 25 to 90 °C (Figure 2d,i, Figure S16a), approaching to the UV−vis results for triblock copolymers in THF (Figure S6). At 70 and 90 °C, the λ_{max} had completely shifted to 445 nm. The blue-shifting of λ_{max} implied that PI_{160}-*b*-$P3HT_{30}$ and PI_{167}-*b*-PS_{42}-*b*-$P3HT_{30}$ were mostly dissolved as unimers. In contrast, the PI_{150}-*b*-PS_{85}-*b*-$P3HT_{30}$ nano-objects required a higher temperature of 90 °C to achieve complete blue-shifting of λ_{max} from 515 to 445 nm (Figure 2e,i) and dissolved as unimers. The longer PS block decreased the solubility of copolymers and weakened the chain mobility, thus increasing the dissolution temperature of PI_{150}-*b*-PS_{85}-*b*-$P3HT_{30}$ in *n*-heptane. Under lower annealing temperatures (25−70 °C), the chain mobility of PI_{150}-*b*-PS_{85}-*b*-$P3HT_{30}$ was restricted and λ_{max} was maintained at 515 nm. For PI_{150}-*b*-PS_{165}-*b*-$P3HT_{30}$ and PI_{135}-*b*-PS_{343}-*b*-$P3HT_{30}$, the λ_{max} dominantly maintained at 515 nm and slight blue-shifting of λ_{max} could be discerned during all annealing temperatures (Figure 2f,i, Figure S16b), demonstrating severely restricted P3HT chain mobility.

Additionally, the nano-objects were also characterized by WAXS analysis. As shown in Figure S15, the nano-objects annealed at 90 °C revealed a progressive attenuation of the (100) ($2\theta = 5.4°$) and (010) ($2\theta = 23.2°$) reflections with the increase of DP_{PS} (Figure S15). Meanwhile, to gain insight into the effect of PS block on the self-assembly, the cloud points of PS homopolymer with different MWs were analyzed in *n*-heptane (containing 1.0% v/v DCM) by performing the UV−vis measurements at 500 nm, while varying the temperatures between 25 ∼ 90 °C by referring to the literature.[47,48] For PS_{42}, the system always had high transmittance over 90% at 500 nm, demonstrating a dissolved state of PS_{42} in *n*-heptane between 25 and 90 °C (Figure S17). For PS_{85}, the system showed an UCST and a phase transition, with a cloud point around 60 °C (Figure S17). For PS_{165} and PS_{343} with higher MWs, both homopolymers had poor solubility between 25 and 90 °C and always had low transmittance below 15%. That is, the PS with higher MWs might have higher phase transition temperatures beyond 90 °C. These results matched well with the above UV−vis results for PI-*b*-PS-*b*-P3HT triblock copolymers, explaining that the P3HT chain mobility at different annealing temperatures was actually influenced by the solvation state of PS block, i.e., the UCST behavior or phase transition of the PS block.

The WAXS, UV−vis results, and cloud point were consistent with those from TEM measurement, confirming that the DP_{PS} was a key modulator in the self-assembly process. With the above results, the self-assembly mechanism of the PI-*b*-PS-*b*-P3HT triblock copolymer is proposed as follows. During the self-assembly process, both crystalline P3HT and amorphous PS formed the core region, and the PI block served as a stabilizer. The self-assembly of PI-*b*-PS-*b*-P3HT with lower DP_{PS} has less dependence on annealing temperatures due to the absence or shortness of the PS block. Once the relatively longer PS was introduced into triblock copolymers, the self-assembly process changed. Accompanying the crystallization of

https://doi.org/10.1021/acs.macromol.5c01262
Macromolecules 2025, 58, 8670−8685

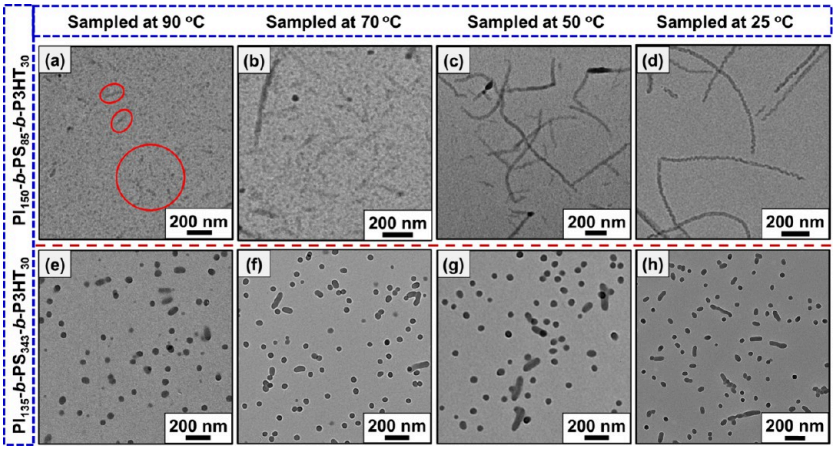

Figure 3. TEM images of nano-objects (diluted into 0.04 mg/mL dispersions) formed by (a–d) PI_{150}-*b*-PS_{85}-*b*-$P3HT_{30}$ and (e–h) PI_{135}-*b*-PS_{343}-*b*-$P3HT_{30}$ in *n*-heptane, annealed at 90 °C, cooled to, and sampled at 90, 70, 50, and 25 °C.

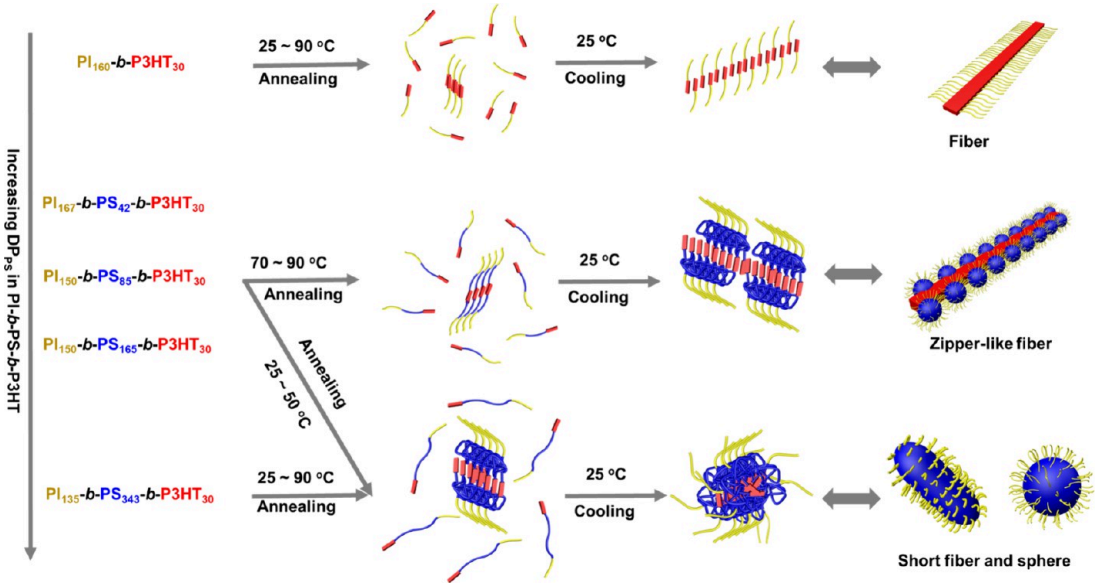

Figure 4. Schematic representation of self-assembly process of PI-*b*-P3HT diblock copolymers and PI-*b*-PS-*b*-P3HT triblock copolymers in *n*-heptane, annealed at different temperatures and cooled to 25 °C.

the P3HT block, the PS block attached and self-assembled on the surface of P3HT, which affected the self-assembly process.

Specifically, after annealing at 90 °C and cooling to 25 °C, for PI_{160}-*b*-$P3HT_{30}$, PI_{167}-*b*-PS_{42}-*b*-$P3HT_{30}$, and PI_{150}-*b*-PS_{85}-*b*-$P3HT_{30}$, the crystallization of the P3HT block preceded the aggregation of the PS block as the moderate PS block could be sufficiently plasticized by *n*-heptane. Thus, the crystallization of the P3HT block dominated the formation of fibers. Uniquely, for PI_{150}-*b*-PS_{85}-*b*-$P3HT_{30}$, the PS block on the surface of the crystalline P3HT core could secondarily self-assemble due to its insolubility under room temperature, causing the zipper-like fibers decorated with serrated edges. To verify the unique self-assembly mechanism, the TEM images of PI_{150}-*b*-PS_{85}-*b*-$P3HT_{30}$ nano-objects annealed at 90 °C, cooled to, and sampled at different temperatures were further monitored and compared. As shown in Figure 3a, only sparse and vague shorter fibers with the length under 50 nm (red circle) could be discriminated at 90 °C. At 70 °C, the fibers became discernible and were lengthened to about 200 nm (Figure 3b). At 50 °C, the longer fibers were clearly observed (Figure 3c) and finally evolved as zipper-like fibers at 25 °C (Figure 3d). Similarly, PI_{150}-*b*-PS_{165}-*b*-$P3HT_{30}$ preferred to form the fibers. However, due to the inadequate stabilization ability of the PI block, the decreased solvation or plasticization of PS block and the inflexibility of the crystalline P3HT, the fibers were unstable and finally precipitated at room temperature (25 °C). As for PI_{135}-*b*-PS_{343}-*b*-$P3HT_{30}$, the solvation or plasticization of the PS block was significantly reduced due to the further increased DP_{PS}. In this case, the solvent-phobicity of the PS block rather than the crystallization of the P3HT block dominated the self-assembly process of the copolymer. The PS covered on the surface of P3HT and interrupted the crystallization of P3HT block, and only the smaller crystalline region could be formed. That is, the preliminary spherical nano-objects hindered the epitaxial growth of P3HT from crystalline core, which finally led to the formation of spheres or short fibers (Figure S18). Obviously, under the same CDSA process, the higher DP_{PS} contributed more effect to the self-assembly process. Again, the conclusion was verified by the TEM images of PI_{135}-*b*-PS_{343}-*b*-$P3HT_{30}$ nano-objects sampled at different temperatures. As shown in Figure 3e–h, the PI_{135}-*b*-PS_{343}-*b*-$P3HT_{30}$ in *n*-heptane self-assembled as spherical

https://doi.org/10.1021/acs.macromol.5c01262
Macromolecules 2025, 58, 8670–8685

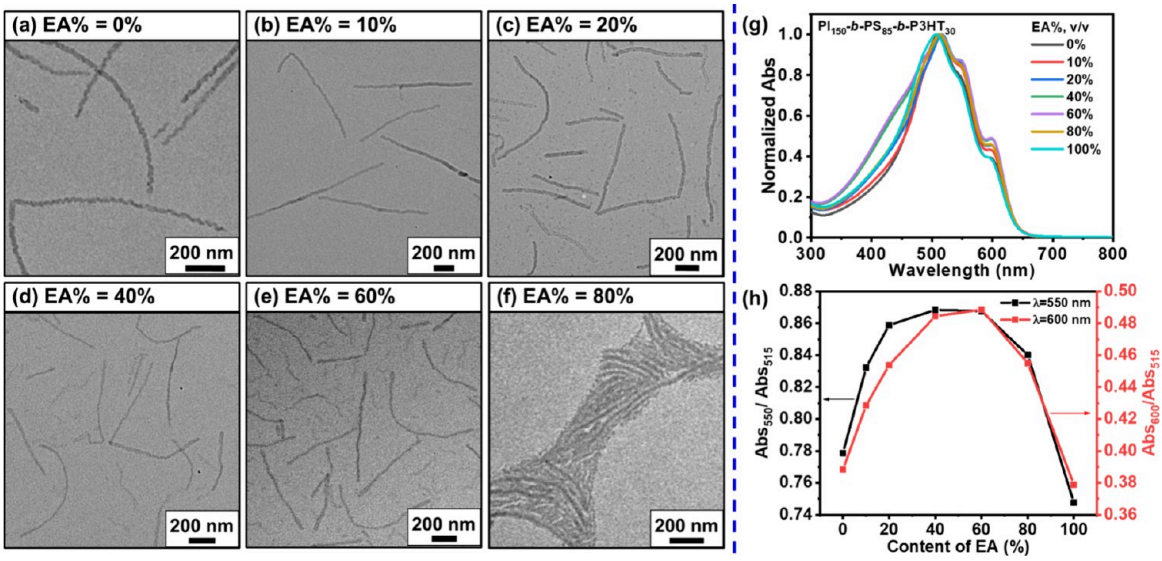

Figure 5. (a–f) TEM images of nano-objects formed by the self-assembly of PI_{150}-*b*-PS_{85}-*b*-$P3HT_{30}$ in Hep/EA cosolvent with different EA%, annealed at 90 °C and sampled at 25 °C. (g) UV–vis spectra for PI_{150}-*b*-PS_{85}-*b*-$P3HT_{30}$ in corresponding cosolvents, annealed at 90 °C and measured at 25 °C. (h) The curves of Abs_{550}/Abs_{515} and Abs_{600}/Abs_{515} for nano-objects.

nano-objects in all temperatures, except that trace of rod-like nano-objects could be observed in the TEM images from relatively lower temperatures.

Alternatively, the relatively lower annealing temperatures (25, 50, and 70 °C) tended to lower the solvation or plasticization of the PS block and accelerated the crystallization of the P3HT block. The contribution of annealing temperatures on the former might weigh over the latter. That is, for the same triblock copolymer, the PS block tended to exert more effect on the self-assembly process at a lower annealing temperature. Especially, the triblock copolymers with higher DP_{PS} were more sensitive to the annealing temperatures. Taken altogether, the solvation or plasticization of the PS block competed with the crystallization of the P3HT block during the cooling process, leading to the formation of unique spheres, zipper-like fibers, or even precipitates as well. The above explanation on self-assembly process of copolymers could be vividly displayed in Figure 4.

Following the above mechanism of self-assembly of copolymers, the evolution of fiber length (Figure 1k) and diameter of spheres of nano-objects (Figure 1l) can also be also explained. For fibrous nano-objects, the lengths were increased regularly with the increase of annealing temperatures (Figure 1k), which followed the typical feature of self-seeding in the CDSA system.[22,29,49] Generally, the copolymers were first dissolved as unimers and dispersed as seed crystalline micelles after being annealed under a certain temperature. Then, the unimers grew onto epitaxial seed crystalline micelles during the cooling process and finally formed the fiber-like structures. Due to the crystallinity of the P3HT block, the process should be modulated by nucleation and growth processes. Comparatively, in the case with relatively higher annealing temperatures, the crystalline micelles were mostly dissolved as unimers, causing less survival of seed crystalline micelles. After a sufficient aging process (also known as the growth process) of 24.0 h, more unimers could grow onto the seed crystalline micelles during the cooling procedure, leading to the formation of longer fibers. Thus, the annealing temperatures have a greater effect on the nucleation process than on the growth process. Furthermore, the PS block affected the widths of fibers or the diameters of spheres, which was increased regularly with the increase of DP_{PS} (Figure 1l). It could be deduced that the PS block with increased DP_{PS} surrounded the P3HT crystal and thickened the outer layer of nano-objects. Intrinsically, the middle PS block tended to disrupt the general fibrous morphology which should be formed by P3HT block under the CDSA system, resulting distinct rearrangement or recrystallization behaviors of the P3HT block in triblock copolymers.

Self-Assembly of PI-*b*-PS-*b*-P3HT Triblock Copolymer in Hep/EA Mixture. Besides the annealing temperatures, the solvents serving as another important parameter could also modulate the morphologies of self-assembled nano-objects. Compared with *n*-heptane, ethyl acetate (EA) was a poorer solvent for P3HT block[50] but a better solvent for PI and PS blocks. Thus, by systematically varying the EA volume fraction (EA%, v/v) in the Hep/EA cosolvent, the self-assembly of triblock copolymers was modulated in an alternative pathway. Following a typical protocol similar to those in *n*-heptane, the PI-*b*-PS-*b*-P3HT triblock copolymers in Hep/EA cosolvent were sequentially annealed at 90 °C for 1.0 h, cooled to 25 °C, and aged for 24 h at a fixed concentration of 0.20 mg/mL.

The reference PI_{160}-*b*-$P3HT_{30}$ diblock copolymer consistently formed fibers in all cosolvent (Figure S19). Differently, the lengths of fibers gradually decreased with the increase of EA% from 0 to 100%. As EA was a poor solvent for P3HT, higher EA% attenuated both the solvation or plasticization of P3HT block, even at the elevated annealing temperature of 90 °C. Consequently, under higher EA%, insufficient molecular rearrangement and recrystallization of the P3HT block resulted in more seed crystalline micelles and fewer unimers being formed, which ultimately yielded shorter fibers. This interpretation was further supported by UV–vis spectra (Figure S20), where the decreasing ratios of Abs_{550}/Abs_{515} and Abs_{600}/Abs_{515} correlated with the diminished reorganization capability of the P3HT block at higher EA%.

Upon the incorporation of the PS_{85} block, PI_{150}-*b*-PS_{85}-*b*-$P3HT_{30}$ self-assembled as zipper-like fibers with an average

https://doi.org/10.1021/acs.macromol.5c01262
Macromolecules 2025, 58, 8670–8685

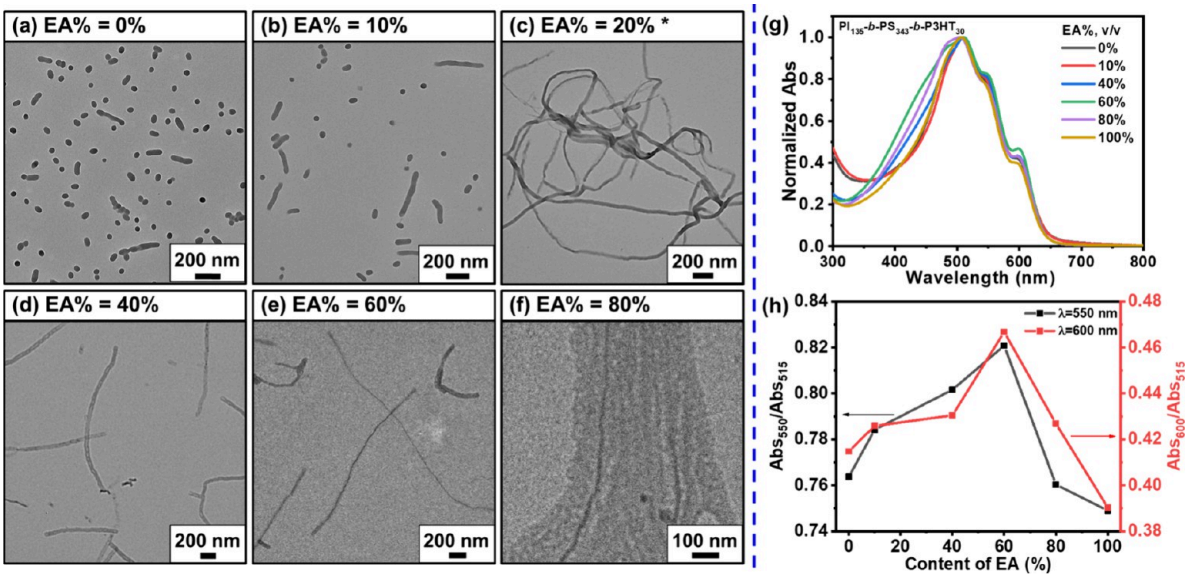

Figure 6. (a–f) TEM images of nano-objects formed by self-assembly of PI_{135}-*b*-PS_{343}-*b*-$P3HT_{30}$ in Hep/EA cosolvents with different EA%, annealed at 90 °C and sampled at 25 °C. (*The nano-objects were annealed at 90 °C and sampled at 45 °C). (g) UV–vis spectra for PI_{135}-*b*-PS_{343}-*b*-$P3HT_{30}$ in corresponding cosolvents, annealed at 90 °C and measured at 25 °C. (h) The curves of Abs_{550}/Abs_{515} and Abs_{600}/Abs_{515} for nano-objects.

width around 30 nm and serrated edges with an average pitch around 15 nm in *n*-heptane (EA% of 0%) as previously described (Figure 5a). Intriguingly, while maintaining fibrous morphology (width of 30 nm) at an EA% of 10–60%, the fibers progressively lost their serrated edges with increasing EA % (Figure 5b–e). At higher EA% (80 and 100%), however, the fibers underwent significant shortening and aggregation (Figure 5f, Figure S21). As analyzed in the above section, the formation of zipper-like fibers in *n*-heptane (EA% of 0%) was attributed to the secondary-assembly of the PS block on the crystalline P3HT core. Increasing EA% enhanced PS solvation or plasticization, transforming its role from core-forming block to stabilizer, thereby eliminating edge serration. Meanwhile, the increase of EA% led to the insufficient rearrangement and recrystallization of the P3HT block, and the shorter fibers were favored. This result represented a morphological evolution from higher-order zipper-like fibers to uniform elongated fibers and finally short fiber aggregates. Notably, in the cloud point experiment, the PS_{85} homopolymer showed a UCST around 60 °C in Hep/EA cosolvent with EA % of 0% and always had high transmittance in Hep/EA cosolvent with EA% above 10% (Figure S22). In the latter case, PS_{85} had good solubility and PS_{85} block in PI_{150}-*b*-PS_{85}-*b*-$P3HT_{30}$ did not have phase separation between 25 and 90 °C, indicating that PS_{85} served as a stabilizer in the self-assembled nano-objects. In this case, the crystallization of P3HT became the dominant driving force, forming the fiber-like structure via the CDSA process. Additionally, the UV–vis spectra revealed maximal Abs_{550}/Abs_{515} and Abs_{600}/Abs_{515} ratios at EA% of 40–60% (Figure 5g,h), indicating optimal chain mobility where reorganization and recrystallization of P3HT block were balanced by the solvation and plasticization effect of PS block.

For PI_{150}-*b*-PS_{165}-*b*-$P3HT_{30}$, the macroscopic precipitates were observed at EA% below 20%. The nano-objects before the precipitation (at 45 °C) were captured as entangled long fibers by TEM measurement (Figure S23a). However, the PI_{150}-*b*-PS_{165}-*b*-$P3HT_{30}$ self-assembled as regular fibers with an EA% of 40 or 60% (Figure S23b,c). Oppositely, the seriously aggregated short fibers could be discriminated with EA% of 80 and 100% (Figure S23d,e). In the cloud point experiment, the PS_{165} homopolymer showed a UCST around 80 °C in Hep/EA cosolvent with EA% of 10% and always had high transmittance in Hep/EA cosolvent with EA% above 20% (Figure S24). That was, in the Hep/EA cosolvent with EA% above 20%, PS_{165} had good solubility and PS_{165} block in PI_{150}-*b*-PS_{85}-*b*-$P3HT_{30}$ did not have phase separation between 25 and 90 °C, serving as a stabilizer in self-assembled nano-objects. Correspondingly, in the cases with EA% of 40 or 60%, the UV–vis spectra showed the maximum Abs_{550}/Abs_{515} and Abs_{600}/Abs_{515} (Figure S25). Thus, the morphological evolution of PI_{150}-*b*-PS_{85}-*b*-$P3HT_{30}$ in Hep/EA cosolvent paralleled the UV–vis spectral changes as well as the cloud points.

For PI_{135}-*b*-PS_{343}-*b*-$P3HT_{30}$ with further increased DP_{PS}, the nano-objects remained as spheres and short fibers with EA% of 0 and 10% (Figure 6a,b). However, the macroscopic precipitation was observed during the cooling process at EA % of 20%, similar to that for PI_{150}-*b*-PS_{165}-*b*-$P3HT_{30}$ at EA% of 0, 10, or 20%. The nano-objects before the precipitation (at 45 °C) were again captured as entangled fibers by TEM measurement (Figure 6c). When EA% was increased to 40 and 60% (Figure 6d,e), the nano-objects evolved into long fibers. The formation of stable dispersions was attributed to the reduced entanglement between nano-objects as the PS block became fully solvated. At EA% of 80% and 100%, however, no regular morphologies could be observed due to the increased solvation or plasticization of the PS_{343} block, and the correspondingly increased length of the PI_{135}-*b*-PS_{343} stabilizer (Figure 6f, Figure S26). For PI_{135}-*b*-PS_{343}-*b*-$P3HT_{30}$, the precipitate only occurred at an EA% of 20% and was avoided at EA% below 10% and above 40%. Compared with PI_{150}-*b*-PS_{165}-*b*-$P3HT_{30}$, the nonequilibrium state was narrowed due to the increased DP_{PS}. With the increases of EA%, the morphologies evolved from lower-order spheres to higher-order long fibers, then to short fibers, and finally to irregular structures. Again, in the cloud point experiment, the PS_{343} homopolymer showed a UCST around 40 °C in Hep/EA

https://doi.org/10.1021/acs.macromol.5c01262
Macromolecules 2025, 58, 8670–8685

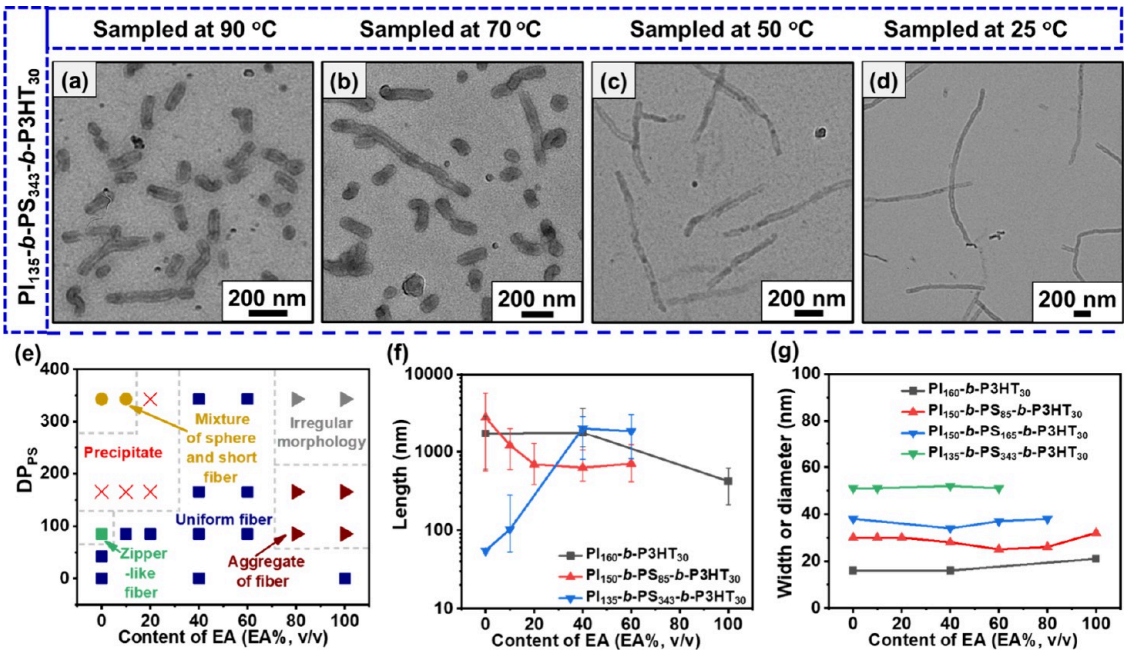

Figure 7. TEM images of nano-objects (diluted into 0.04 mg/mL dispersions) formed by PI_{135}-*b*-PS_{343}-*b*-$P3HT_{30}$ in Hep/EA cosolvent with EA% of 40%, annealed at 90 °C, cooled to, and sampled at (a) 90 °C, (b) 70 °C, (c) 50 °C, and (d) 25 °C. (e) The morphology diagram of nano-objects based on the relationship of DP_{PS} with EA%. (f) Length of fibers vs EA%. (g) Width or diameter of nano-objects vs EA%.

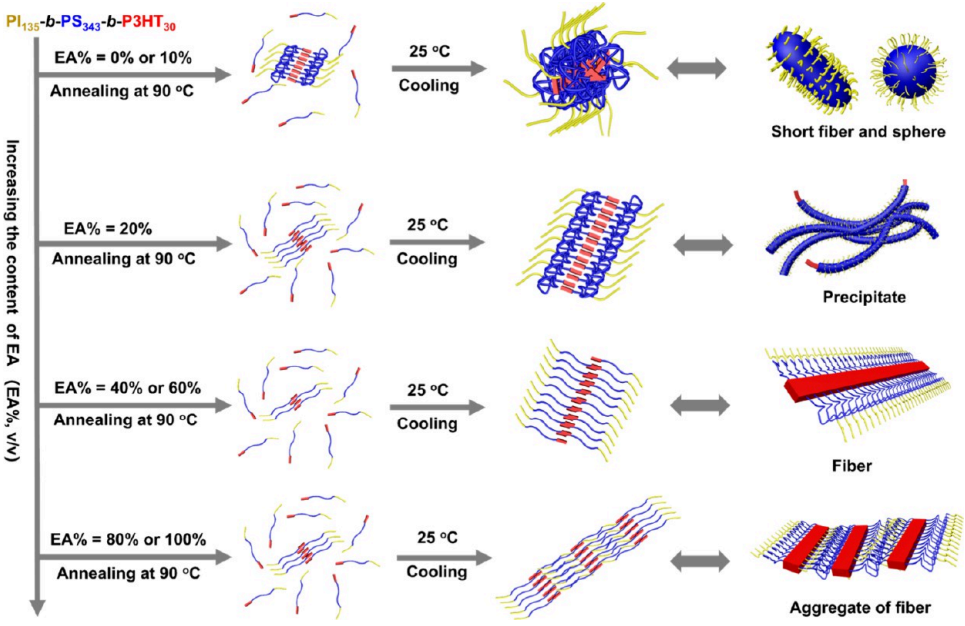

Figure 8. Schematic representation of the self-assembly process of PI_{135}-*b*-PS_{343}-*b*-$P3HT_{30}$ in Hep/EA cosolvent with different EA%, annealed at 90 °C, and cooled to 25 °C.

cosolvent with EA% of 30% and always had high transmittance in Hep/EA cosolvent with EA% above 40% (Figure S27). In Hep/EA cosolvent with EA% above 40%, PS_{343} had good solubility and PS_{343} block in PI_{135}-*b*-PS_{343}-*b*-$P3HT_{30}$ did not have phase separation between 25 and 90 °C, changing from the role of core-forming block to a stabilizer in self-assembled nano-objects. Similarly, at an EA% of 40%, the UV−vis spectra showed maximum Abs_{550}/Abs_{515} and Abs_{600}/Abs_{515} ratios (Figure 6g,h). Additionally, from the WAXS diffraction pattern, the (100) reflection peak at 2θ = 5.4° for PI_{135}-*b*-PS_{343}-*b*-$P3HT_{30}$ could be clearly observed at the EA% of 0, 40, and 60%. However, the diffraction pattern completely disappeared at an EA% of 100% (Figure S28), indicating the loss of the P3HT block crystallization due to the increased solvation or plasticization of the PS_{343} block and the extended length of the PI_{135}-*b*-PS_{343} stabilizer.

Furthermore, to gain insight into the morphological evolution in the Hep/EA cosolvent, the TEM images of PI_{135}-*b*-PS_{343}-*b*-$P3HT_{30}$ nano-objects annealed at 90 °C and sampled at different temperatures in Hep/EA (EA% = 40%) were further monitored and compared with those in *n*-heptane (EA% = 0%). As previously mentioned, the PI_{135}-*b*-PS_{343}-*b*-

https://doi.org/10.1021/acs.macromol.5c01262
Macromolecules 2025, 58, 8670−8685

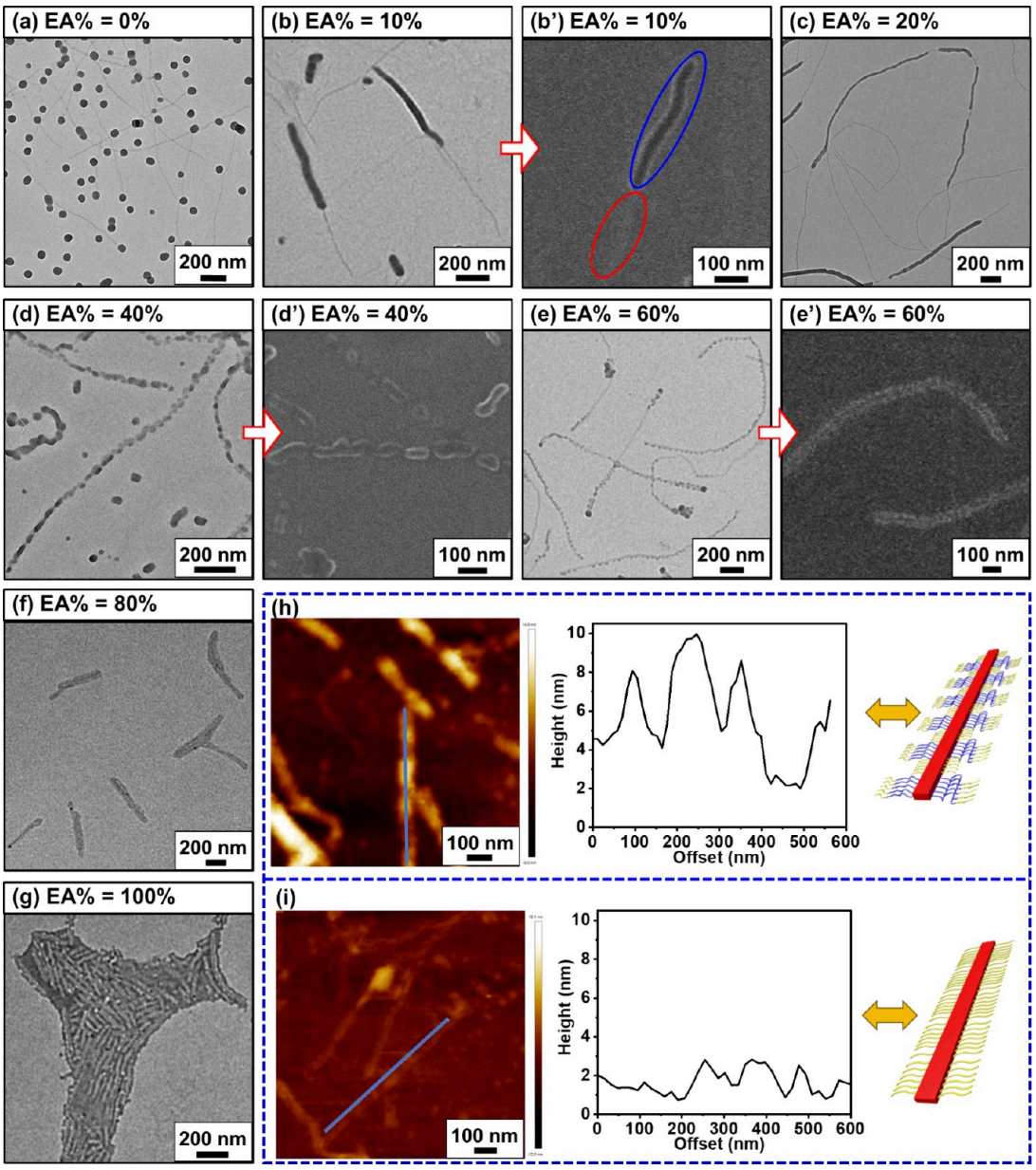

Figure 9. TEM images of nano-objects formed by self-assembly of PI_{160}-*b*-$P3HT_{30}$/PI_{135}-*b*-PS_{343}-*b*-$P3HT_{30}$ in Hep/EA cosolvent with EA% of (a) 0%, (b) 10%, (c) 20%, (d) 40%, (e) 60%, (f) 80%, and (g) 100%, annealed at 90 °C and sampled at 25 °C. SEM images of nano-objects in Hep/EA cosolvent with different EA% of (b′) 10%, (d′) 40%, and (e′) 60%. AFM image and high profile of nano-objects of (h) PI_{160}-*b*-$P3HT_{30}$/PI_{135}-*b*-PS_{343}-*b*-$P3HT_{30}$ with EA% of 40% and (i) PI_{160}-*b*-$P3HT_{30}$ with EA% of 0%.

$P3HT_{30}$ self-assembled as spherical nano-objects in *n*-heptane at 90, 70, 50, and 25 °C, respectively (Figure 3e−h). Differently, at an EA% of 40%, the cloud point experiment indicated that the PS_{343} block had been dissolved and evolved as a stabilizer (Figure S27). In this case, the PI_{135}-*b*-PS_{343}-*b*-$P3HT_{30}$ formed fibers with a length of 100−400 nm at 90 and 70 °C, which was just driven by the crystallization of P3HT block, rather than the phase separation of PS block (Figure 7a,b). Although the fibers were stubby, the high-contrast P3HT core could be clearly observed along the central axis of the fiber, while the gray regions corresponded to the PI_{135}-*b*-PS_{343} shell. Additionally, the fibers were lengthened to 600−2500 nm when cooled to 50 and 25 °C (Figure 7c,d), consistent with the typical CDSA process.

Based on the TEM results, the morphology diagram under the relationship between the DP_{PS} and EA% was depicted and shown in Figure 7e. According to the diagram, the PI-*b*-PS-*b*-P3HT triblock copolymers could form fibers in the case with lower DP_{PS} and EA%, aggregate or irregular morphology in the case with higher DP_{PS} and EA%, spheres and short fibers in the case with higher DP_{PS} and lower EA%. Occasionally, the precipitates could result due to the loss of equilibrium between the solvation or plasticization of the PS block and the crystallization of the P3HT block. That is, these results could be attributed to cooperative self-assembly of the introduced PS with the P3HT blocks. Unlike the above relationship between length of fibers with annealing temperatures in *n*-heptane (Figure 1k), the dependence of fiber length on EA% became complicated. For PI_{160}-*b*-$P3HT_{30}$ and PI_{150}-*b*-PS_{85}-*b*-$P3HT_{30}$, the fiber length decreased with the increase of EA% (Figure 7f). However, for PI_{135}-*b*-PS_{343}-*b*-$P3HT_{30}$, the fiber length regularly increased with increasing EA% (Figure 7f). The

https://doi.org/10.1021/acs.macromol.5c01262
Macromolecules 2025, 58, 8670−8685

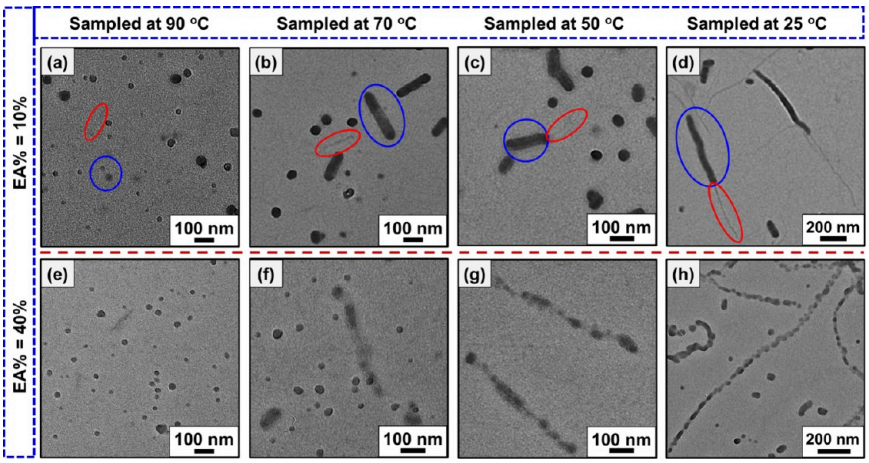

Figure 10. TEM images of nano-objects formed by self-assembly of PI_{160}-*b*-$P3HT_{30}$/PI_{135}-*b*-PS_{343}-*b*-$P3HT_{30}$ in Hep/EA cosolvent with EA% of (a–d) 10% and (e–h) 40%, annealed at 90 °C, cooled to, and sampled at 90, 70, 50, and 25 °C, respectively.

reason might be attributed to the comprehensive effect of the annealing temperature, DP_{PS} and EA%. The EA% acted as an alternative factor to modulate the solvation or plasticization of the PS block and the crystallization of the P3HT block. Regarding the dependence of width of the fibers or the diameter of spheres on DP_{PS}, the similar results to those in Figure 1l were collected. Again, the dependence had less connection with EA%, while maintaining a strong correlation with DP_{PS} (Figure 7g). Thus, comprehensive analysis on the TEM, UV–vis, WAXS results, and cloud point in cosolvent further suggested that the self-assembly process was synergistically coordinated by the solvation or plasticization of the PS block and crystallization of the P3HT block, rather than being dominated by either factor alone. Correspondingly, the self-assembly process in different EA% could be illustrated as in Figure 8.

Cooperative Self-Assembly of Binary PI-*b*-PS-*b*-P3HT Triblock Copolymers in Hep/EA Mixture. Cooperatively self-assembly of different copolymers, serving as an alternative pathway, can be used to generate the compositionally and geometrically complex nano-objects.[51−54] Based on the above results, different PI-*b*-PS-*b*-P3HT copolymers were equimolarly blended, and the cooperative self-assembly was also investigated.

The PI_{160}-*b*-$P3HT_{30}$ and PI_{135}-*b*-PS_{343}-*b*-$P3HT_{30}$ were first mixed in *n*-heptane (EA% of 0%). As shown in Figure 9a, the spherical nano-objects formed by PI_{135}-*b*-PS_{343}-*b*-$P3HT_{30}$ and the uniform fibers formed by PI_{160}-*b*-$P3HT_{30}$ were clearly distinguished. In a previous section, it has been inferred that the solvation or plasticization of the PS_{343} block was the dominant driving-force for PI_{135}-*b*-PS_{343}-*b*-$P3HT_{30}$ in *n*-heptane. For PI_{160}-*b*-$P3HT_{30}$, the rearrangement or recrystallization of $P3HT_{30}$ block was the driving-force. Thus, due to the incompatibility between core-forming PS and P3HT blocks,[55,56] the self-assembly behavior of PI_{160}-*b*-$P3HT_{30}$ and PI_{135}-*b*-PS_{343} was completely different and occurred independently in the same solvent of *n*-heptane (Figure S29). When the EA% was increased to 10%, the solvation or plasticization of the PS_{343} block was improved, leading to the fusion between PI_{135}-*b*-PS_{343}-*b*-$P3HT_{30}$ and PI_{160}-*b*-$P3HT_{30}$. Unlike the smooth and uniform fibers formed from PI_{160}-*b*-$P3HT_{30}$ in Figure 1c, some fibers with a thinner width around 14 nm and a thicker width around 50 nm generated by PI_{160}-*b*-$P3HT_{30}$ (red circle) and PI_{135}-*b*-PS_{343}-*b*-$P3HT_{30}$ (blue circle), respectively, were connected, forming the block-like fibers (Figure 9b,b′). At an EA% of 20%, the length of the block-like fibers was further increased (Figure 9c). Unlike the precipitate formed by PI_{135}-*b*-PS_{343}-*b*-$P3HT_{30}$ at an EA% of 20% in Figure 6c, the nano-objects generated from the mixture of PI_{160}-*b*-$P3HT_{30}$ and PI_{135}-*b*-PS_{343}-*b*-$P3HT_{30}$ remained stable for several days without precipitation. Furthermore, at EA% of 40 and 60%, the bead-like fibers were presented (Figure 9d,e). The SEM images showed a rough surface on the nano-objects (Figure 9d′,e′). The AFM analysis displayed clear axial height fluctuations in individual nano-objects, confirming the formation of a bead-like fibrous structure at an EA% of 40% (Figure 9h). Comparatively, the height profile of bead-like fibers was completely different from that of PI_{160}-*b*-$P3HT_{30}$-based uniform fibers in *n*-heptane (Figure 9i), which exhibited a smooth surface and weak height fluctuation. Thus, it was proposed that the bead-like fibers consist of the alternation of thinner fiber of PI_{160}-*b*-$P3HT_{30}$ and thicker fiber of PI_{135}-*b*-PS_{343}-*b*-$P3HT_{30}$. Further, when EA% was increased to 80 and 100%, the fibers became short (Figure 9f) and tended to aggregate (Figure 9g). In this case, as the PI_{135}-*b*-PS_{343} acted as the similar stabilizer function as that by PI_{160}, the PI_{160}-*b*-$P3HT_{30}$ and PI_{135}-*b*-PS_{343}-*b*-$P3HT_{30}$ were completely fused and coassembled. Thus, the morphological evolution at EA% from 0 to 100% confirmed that cooperative effects did occur between PI_{160}-*b*-$P3HT_{30}$ and PI_{135}-*b*-PS_{343}-*b*-$P3HT_{30}$.

To disclose the formation mechanism of the unique block-like and bead-like fibers, the TEM images of PI_{160}-*b*-$P3HT_{30}$/PI_{135}-*b*-PS_{343}-*b*-$P3HT_{30}$ in EA% of 10 and 40% were further monitored by annealing at 90 °C and sampling at different temperatures. At an EA% of 10%, PI_{160}-*b*-$P3HT_{30}$/PI_{135}-*b*-PS_{343}-*b*-$P3HT_{30}$ formed a mixture of short fibers (red circle) and spheres (blue circle) at 90 °C (Figure 10a). Decreasing the sampling temperature to 70 °C, these two nano-objects independently grew and lengthened, while maintaining their separate morphologies (Figure 10b). Further decreased the sampling temperature was further decreased to 50 °C, some of the fibers and sphere merged, forming the block-like fibers (Figure 10c). Finally, at 25 °C, more block-like fibers were collected, and the length was further increased (Figure 10d). Alternatively, increasing the EA% to 40%, the PI_{160}-*b*-$P3HT_{30}$/PI_{135}-*b*-PS_{343}-*b*-$P3HT_{30}$ also formed short fibers and spheres at 90 °C (Figure 10e), similar to the case with an EA% of 10%. However, at 70 °C, the bead-like fibers could be discriminated

https://doi.org/10.1021/acs.macromol.5c01262
Macromolecules 2025, 58, 8670−8685

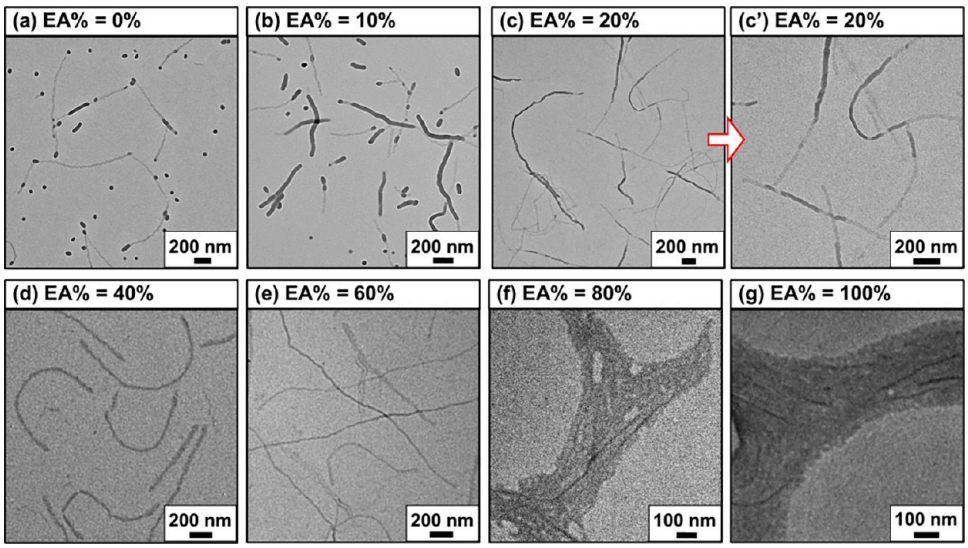

Figure 11. TEM images of nano-objects formed by self-assembly of PI_{150}-*b*-PS_{85}-*b*-$P3HT_{30}$/PI_{135}-*b*-PS_{343}-*b*-$P3HT_{30}$ in Hep/EA cosolvent with different EA%s of (a) 0%, (b) 10%, (c, c′) 20%, (d) 40%, (e) 60%, (f) 80% and (g) 100%, annealed at 90 °C and sampled at 25 °C.

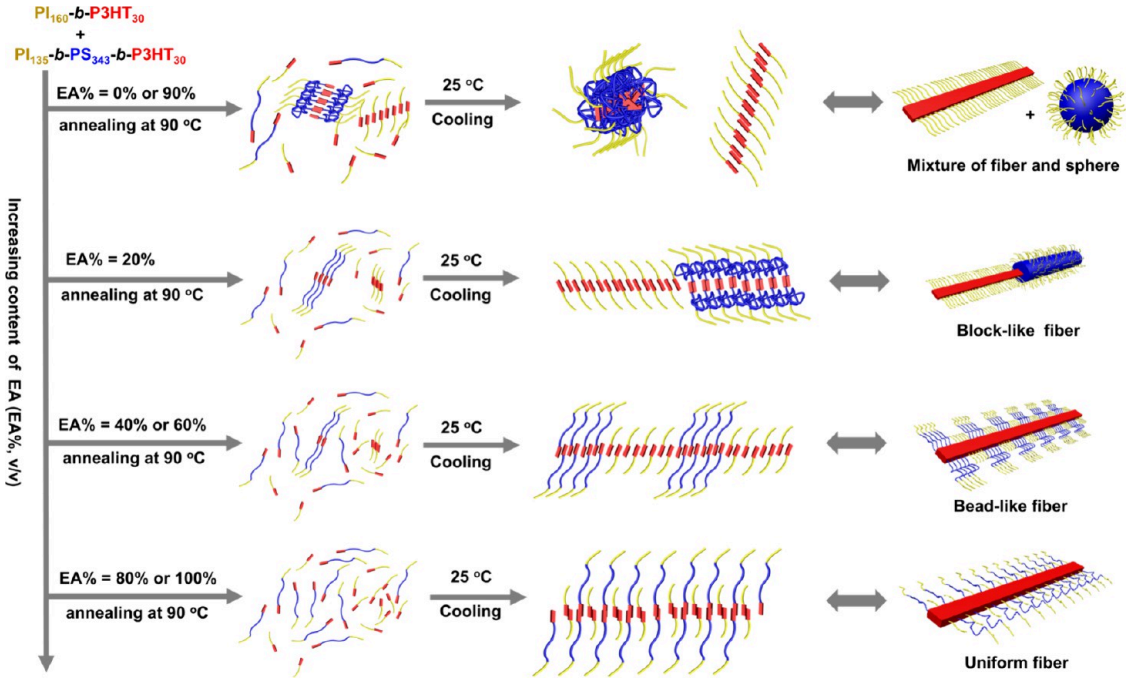

Figure 12. Schematic representation of cooperative self-assembly process of PI_{160}-*b*-$P3HT_{30}$/PI_{135}-*b*-PS_{343} in Hep/EA cosolvent with different EA %, annealed at 90 °C and cooled to 25 °C.

(Figure 10f), where the intermediate was discerned by two kinds of dissolved unimers gluing onto the seed micelles alternately. Continuously, the bead-like fibers were further lengthened at a lower sampling temperature of 50 and 25 °C (Figure 10g,h). Obviously, these results indicated that the coassembly mechanism was different in the cases with an EA% of 10 and 40%. That is, the PI_{160}-*b*-$P3HT_{30}$/PI_{135}-*b*-PS_{343}-*b*-$P3HT_{30}$ formed block-like fibers via direct mergence of two fiber-like micelles at EA% of 10%, while it formed bead-like fibers through the similar seeded growth of CDSA at an EA% of 40%.

Alternatively, the cooperative self-assembly processes of PI_{150}-*b*-PS_{85}-*b*-$P3HT_{30}$ and PI_{135}-*b*-PS_{343}-*b*-$P3HT_{30}$ were also studied. The TEM image showed a mixture of spheres and fibers, accompanying block-like fibers with a thinner width (30 nm) and a thicker width (50 nm), in *n*-heptane (EA% of 0%) (Figure 11a). When EA% was increased to 10 and 20%, more block-like fibers were available (Figure 11b,c,c′). At an EA% of 40 and 60%, the copolymers were completely fused and cooperatively self-assembled as uniform fibers with smooth surfaces and homogeneous contour (Figure 11d,e). At an EA% of 80% (Figure 11f) and 100% (Figure 11g), the higher EA% led to the formation of aggregates with a vague contour due to the sufficient solvation of PI_{150}-*b*-PS_{85} and PI_{135}-*b*-PS_{343} stabilizers.

The results from the cooperative self-assembly of different copolymers further indicated that the PS block played an important role in the self-assembly process. The PI_{160}-*b*-

https://doi.org/10.1021/acs.macromol.5c01262
Macromolecules 2025, 58, 8670−8685

$P3HT_{30}$ diblock copolymer could not cooperatively self-assemble with PI_{135}-*b*-PS_{343}-*b*-$P3HT_{30}$ in *n*-heptane (EA% of 0%). With the addition of ethyl acetate, the PS gradually became a soluble block and stabilizer block, leading to the self-assembly with different mechanisms at EA% of 10 and 40%, and the complete fusion between PI_{160}-*b*-$P3HT_{30}$ and PI_{135}-*b*-PS_{343}-*b*-$P3HT_{30}$ at EA% of 80% (Figure 12). Alternatively, PI_{150}-*b*-PS_{85}-*b*-$P3HT_{30}$, even with a relatively shorter PS_{85}, could greatly promote complete fusion with PI_{135}-*b*-PS_{343}-*b*-$P3HT_{30}$ at a relatively lower EA% of 40%. Compared with the mixture of PI_{160}-*b*-$P3HT_{30}$ and PI_{135}-*b*-PS_{343}-*b*-$P3HT_{30}$, the complete fusion of PI_{150}-*b*-PS_{85}-*b*-$P3HT_{30}$ and PI_{135}-*b*-PS_{343}-*b*-$P3HT_{30}$ happened at relatively lower EA%. The affinity between PS_{85} and PS_{343} could be attributed to the major reason. Thus, the cooperative self-assembly also served as an efficient route to modulate the morphologies of nano-objects.

CONCLUSIONS

In summary, the PI-*b*-PS-*b*-P3HT triblock copolymers with relatively fixed DP_{PI} and DP_{P3HT}, but different DP_{PS}, were synthesized and self-assembled. First, in *n*-heptane, the relatively lower DP_{PS} and higher annealing temperatures facilitated the formation of uniform fibers, while the higher DP_{PS} and lower annealing temperatures favored the formation of spheres. Second, the self-assembly mechanism was probed by analyzing the UV−vis spectra, from which the λ_{max}, Abs_{550}/Abs_{515}, and Abs_{600}/Abs_{515} could be derived and compared. Subsequently, under an annealing temperature of 90 °C, lower DP_{PS} and lower EA% promoted the formation of long fibers, while other conditions favored the formation of spheres, short fibers, aggregate of fibers, or precipitates. Finally, cooperative self-assembly was also verified as an alternative route to modulate the morphologies of nano-objects. Under all conditions, the morphological evolution was explained by the balance between the solvation or plasticization of the middle PS block and rearrangement or recrystallization of the end P3HT block. Besides the typical uniform fibers, the rarely reported spheres, zipper-like fibers, block-like fibers, bead-like fibers, were also fabricated by optimizing the annealing temperatures, cosolvents, as well as the cooperative self-assembly, which greatly broadened the morphology diagram window. With these results, it was confirmed that the PS block played important roles in the self-assembly of the PI-*b*-PS-*b*-P3HT triblock copolymers. This work provides further insight into the self-assembly technique, especially, which greatly facilitated the preparation of nano-objects containing π-conjugated polymers and their applications.

ASSOCIATED CONTENT

Supporting Information

The Supporting Information is available free of charge at https://pubs.acs.org/doi/10.1021/acs.macromol.5c01262.

Experimental procedures for the synthesis and additional characterization data, including Figures S1−S24 and Table S1 (PDF)

AUTHOR INFORMATION

Corresponding Author

Guowei Wang − *State Key Laboratory of Molecular Engineering of Polymers, Department of Macromolecular Science, Fudan University, Shanghai 200433, China;* orcid.org/0000-0003-2595-8269; Email: gwwang@fudan.edu.cn

Authors

Boyang Shi − *State Key Laboratory of Molecular Engineering of Polymers, Department of Macromolecular Science, Fudan University, Shanghai 200433, China*

Ding Shen − *State Key Laboratory of Molecular Engineering of Polymers, Department of Macromolecular Science, Fudan University, Shanghai 200433, China*

Jingwei Zhang − *State Key Laboratory of Molecular Engineering of Polymers, Department of Macromolecular Science, Fudan University, Shanghai 200433, China*

Xiaoxiao Wu − *State Key Laboratory of Molecular Engineering of Polymers, Department of Macromolecular Science, Fudan University, Shanghai 200433, China*

Chengguang Liu − *State Key Laboratory of Molecular Engineering of Polymers, Department of Macromolecular Science, Fudan University, Shanghai 200433, China*

Complete contact information is available at: https://pubs.acs.org/10.1021/acs.macromol.5c01262

Notes

The authors declare no competing financial interest.

ACKNOWLEDGMENTS

We appreciate the financial support of this research by the National Natural Science Foundation of China (22271058).

REFERENCES

(1) Nketia-Yawson, B.; Ahn, H.; Jo, J. W. Understanding Effects of Ion Diffusion on Charge Carrier Mobility of Electrolyte-Gated Organic Transistor Using Ionic Liquid-Embedded Poly(3-hexylthiophene). *Adv. Funct. Mater.* **2022**, *32* (2), 2108215.

(2) Persson, N. E.; Chu, P. H.; McBride, M.; Grover, M.; Reichmanis, E. Nucleation, Growth, and Alignment of Poly(3-hexylthiophene) Nanofibers for High-Performance OFETs. *Acc. Chem. Res.* **2017**, *50* (4), 932−942.

(3) Cheng, S.; Wang, Y. F.; Zhang, R. S.; Wang, H. J.; Sun, C. F.; Wang, T. Recent Progress in Gas Sensors Based on P3HT Polymer Field-Effect Transistors. *Sensors-Basel* **2023**, *23* (19), 8309.

(4) Feng, X. F.; Zhao, W.; Ju, H. X.; Zhang, L.; Ye, Y. F.; Zhang, W. H.; Zhu, J. F. Electronic structures and chemical reactions at the interface between Li and regioregular poly (3-hexylthiophene). *Org. Electron* **2012**, *13* (6), 1060−1067.

(5) Borriello, C.; Masala, S.; Bizzarro, V.; Nenna, G.; Re, M.; Pesce, E.; Minarini, C.; Di Luccio, T. Electroluminescence Properties of Poly(3-hexylthiophene)-Cadmium Sulfide Nanoparticles Grown. *J. Appl. Polym. Sci.* **2011**, *122* (6), 3624−3629.

(6) Ostergard, T.; Pal, A. J.; Paloheimo, J.; Stubb, H. Light-emitting diodes of poly(3-hexylthiophene) Langmuir-Blodgett films. *Synth. Met.* **1997**, *85* (1−3), 1249−1250.

(7) Chatterjee, S.; Jinnai, S.; Ie, Y. Nonfullerene acceptors for P3HT-based organic solar cells. *J. Mater. Chem. A* **2021**, *9* (35), 18857−18886.

(8) Xian, K.; Ma, R.; Zhou, K.; Liu, J.; Gao, M.; Zhao, W.; Li, M.; Geng, Y.; Ye, L. Miscibility screening promotes the efficiency and stability of P3HT-based organic solar cells. *Aggregate* **2024**, *5*, No. e466.

(9) Chang, B.; Chen, C. H.; Hsueh, T. F.; Tan, S.; Lin, Y. C.; Zhao, Y.; Tsai, B. S.; Chu, T. Y.; Chang, Y. N.; Tsai, C. E.; Chen, C. S.; Wei, K. H.; et al. High-Performance Poly(3-hexyl thiophene)-Based Organic Photovoltaics with Side-Chain Engineering of Core Units of Small Molecule Acceptors. *ACS Appl. Mater. Interfaces* **2023**, *15* (45), 52651−52660.

(10) Ludwigs, S.*P3HT Revisited - from Molecular Scale to Solar Cell Devices Preface*; Springer 2014.
(11) Poelking, C.; Andrienko, D. Effect of Polymorphism, Regioregularity and Paracrystallinity on Charge Transport in Poly(3-hexylthiophene) [P3HT] Nanofibers. *Macromolecules* **2013**, *46* (22), 8941−8956.
(12) Cho, S.; Lee, K.; Yuen, J.; Wang, G.; Moses, D.; Heeger, A. J.; Surin, M.; Lazzaroni, R. Thermal annealing-induced enhancement of the field-effect mobility of regioregular poly(3-hexylthiophene) films. *J. Appl. Phys.* **2006**, *100*, No. 114503.
(13) Yuan, Y.; Zhang, J. M.; Sun, J. Q.; Hu, J.; Zhang, T. P.; Duan, Y. X. Polymorphism and Structural Transition around 54 °C in Regioregular Poly(3-hexylthiophene) with High Crystallinity as Revealed by Infrared Spectroscopy. *Macromolecules* **2011**, *44* (23), 9341−9350.
(14) Yu, X.; Xiao, K.; Chen, J.; Lavrik, N. V.; Hong, K.; Sumpter, B. G.; Geohegan, D. B. High-Performance Field-Effect Transistors Based on Polystyrene-*b*-Poly(3-hexylthiophene) Diblock Copolymers. *ACS Nano* **2011**, *5* (5), 3559−3567.
(15) Chevrier, M.; Lopez, G.; Zajaczkowski, W.; Kesters, J.; Lenaerts, R.; Surin, M.; De Winter, J.; Richeter, S.; Pisula, W.; Mehdi, A.; et al. Synthesis and properties of a P3HT-based ABA triblock copolymer containing a perfluoropolyether central segment. *Synth. Met.* **2019**, *252*, 127−134.
(16) Fujita, H.; Michinobu, T.; Tokita, M.; Ueda, M.; Higashihara, T. Synthesis and Postfunctionalization of Rod-Coil Diblock and Coil-Rod-Coil Triblock Copolymers Composed of Poly(3-hexylthiophene) and Poly(4-(4′-N,N-dihexylaminophenylethynyl)styrene) Segments. *Macromolecules* **2012**, *45* (24), 9643−9656.
(17) Peng, R.; Pang, B.; Hu, D. Q.; Chen, M. J.; Zhang, G. B.; Wang, X. H.; Lu, H. B.; Cho, K.; Qiu, L. Z. An ABA triblock copolymer strategy for intrinsically stretchable semiconductors. *J. Mater. Chem. C* **2015**, *3* (15), 3599−3606.
(18) Higashihara, T.; Fukuta, S.; Ochiai, Y.; Sekine, T.; Chino, K.; Koganezawa, T.; Osaka, I. Synthesis and Deformable Hierarchical Nanostructure of Intrinsically Stretchable ABA Triblock Copolymer Composed of Poly(3-hexylthiophene) and Polyisobutylene Segments. *ACS Appl. Polym. Mater.* **2019**, *1* (3), 315−320.
(19) Le Nguyen, T. P.; Bui, T. T.; Nguyen, C. H. T.; Le, D. T.; Nguyen, T. H.; Nguyen, L. T. T.; Nguyen, Q. T.; Hoang, M. H.; Yokozawa, T.; Nguyen, H. T. Diblock copolymers poly(3-hexylthiophene)-block-poly(2-(dimethylamino)ethyl methacrylate-*random*-1-pyrenylmethyl methacrylate), controlled synthesis and optical properties. *J. Polym. Res.* **2023**, *30* (8), 292.
(20) Yang, W.; Lin, Y.; Inagaki, S.; Shimizu, H.; Ercan, E.; Hsu, L.; Chueh, C.; Higashihara, T.; Chen, W. Low-Energy-Consumption and Electret-Free Photosynaptic Transistor Utilizing Poly(3-hexylthiophene)-Based Conjugated Block Copolymers. *Adv. Sci.* **2022**, *9* (8), 2105190.
(21) Zheng, Q. B.; Lin, Y. C.; Lin, Y. T.; Chang, Y.; Wu, W. N.; Lin, J. M.; Tung, S. H.; Chen, W. C.; Liu, C. L. Investigating the stretchability of doped poly(3-hexylthiophene)-block-poly (butyl acrylate) conjugated block copolymer thermoelectric thin films. *Chem. Eng. J.* **2023**, *472*, No. 145121.
(22) Shi, B.; Shen, D.; Li, W.; Wang, G. Self-Assembly of Copolymers Containing Crystallizable Blocks: Strategies and Applications. *Macromol. Rapid Commun.* **2022**, *43* (14), 2200071.
(23) MacFarlane, L.; Zhao, C. Q.; Cai, J. D.; Qiu, H. B.; Manners, I. Emerging applications for living crystallization-driven self-assembly. *Chem. Sci.* **2021**, *12* (13), 4661−4682.
(24) Ma, J. Y.; Lu, G. L.; Huang, X. Y.; Feng, C. π-Conjugated-polymer-based nanofibers through living crystallization-driven self-assembly: preparation, properties and applications. *Chem. Commun.* **2021**, *57* (98), 13259−13274.
(25) Yang, H.; Xia, H.; Wang, G. W.; Peng, J.; Qiu, F. Insights into poly(3-hexylthiophene)-*b*-poly(ethylene oxide) block copolymer: Synthesis and solvent-induced structure formation in thin films. *J. Polym. Sci., Part A:Polym. Chem.* **2012**, *50* (24), 5060−5067.
(26) Gwyther, J.; Gilroy, J. B.; Rupar, P. A.; Lunn, D. J.; Kynaston, E.; Patra, S. K.; Whittell, G. R.; Winnik, M. A.; Manners, I. Dimensional Control of Block Copolymer Nanofibers with a -Conjugated Core: Crystallization-Driven Solution Self-Assembly of Amphiphilic Poly(3-hexylthiophene)-*b*-poly(2-vinylpyridine). *Chem. - Eur. J.* **2013**, *19* (28), 9186−9197.
(27) Patra, S. K.; Ahmed, R.; Whittell, G. R.; Lunn, D. J.; Dunphy, E. L.; Winnik, M. A.; Manners, I. Cylindrical Micelles of Controlled Length with a pi-Conjugated Polythiophene Core via Crystallization-Driven Self-Assembly. *J. Am. Chem. Soc.* **2011**, *133* (23), 8842−8845.
(28) Gilroy, J. B.; Lunn, D. J.; Patra, S. K.; Whittell, G. R.; Winnik, M. A.; Manners, I. Fiber-like Micelles via the Crystallization-Driven Solution Self-Assembly of Poly(3-hexylthiophene)-*block*-Poly(methyl methacrylate) Copolymers. *Macromolecules* **2012**, *45* (14), 5806−5815.
(29) Qian, J. S.; Li, X. Y.; Lunn, D. J.; Gwyther, J.; Hudson, Z. M.; Kynaston, E.; Rupar, P. A.; Winnik, M. A.; Manners, I. Uniform, High Aspect Ratio Fiber-like Micelles and Block Co-micelles with a Crystalline pi-Conjugated Polythiophene Core by Self-Seeding. *J. Am. Chem. Soc.* **2014**, *136* (11), 4121−4124.
(30) Li, X.; Wolanin, P. J.; MacFarlane, L. R.; Harniman, R. L.; Qian, J.; Gould, O. E. C.; Dane, T. G.; Rudin, J.; Cryan, M. J.; Schmaltz, T.; Frauenrath, H.; Winnik, M. A.; Faul, C. F. J.; Manners, I.; et al. Uniform electroactive fibre-like micelle nanowires for organic electronics. *Nat. Commun.* **2017**, *8*, 16142.
(31) Fukui, T.; Garcia-Hernandez, J. D.; MacFarlane, L. R.; Lei, S. X.; Whittell, G. R.; Manners, I. Seeded Self-Assembly of Charge-Terminated Poly(3-hexylthiophene) Amphiphiles Based on the Energy Landscape. *J. Am. Chem. Soc.* **2020**, *142* (35), 15038−15048.
(32) MacFarlane, L. R.; Li, X. Y.; Faul, C. F. J.; Manners, I. Efficient and Controlled Seeded Growth of Poly(3-hexylthiophene) Block Copolymer Nanofibers through Suppression of Homogeneous Nucleation. *Macromolecules* **2021**, *54* (24), 11269−11280.
(33) Reichstein, P. M.; Gödrich, S.; Papastavrou, G.; Thelakkat, M. Influence of Composition of Amphiphilic Double-Crystalline P3HT-*b*-PEG Block Copolymers on Structure Formation in Aqueous Solution. *Macromolecules* **2016**, *49* (15), 5484−5493.
(34) Qi, R.; Zhu, Y. L.; Han, L.; Wang, M. J.; He, F. Rectangular Platelet Micelles with Controlled Aspect Ratio by Hierarchical Self-Assembly of Poly(3-hexylthiophene)-*b*-poly(ethylene glycol). *Macromolecules* **2020**, *53* (15), 6555−6565.
(35) Kang, S.; Kim, G. H.; Park, S. J. Conjugated Block Copolymers for Functional Nanostructures. *Acc. Chem. Res.* **2022**, *55* (16), 2224−2234.
(36) Zhang, H. R.; Heng, Z. G.; Zhou, J.; Shen, L.; Chen, Y.; Zou, H. W.; Liang, M. Robust organic semiconductor thermoset composite films based on Crystallization-Driven Self-Assembled nanofibers of Poly (3-hexylthiophene) block copolymers. *Chem. Eng. J.* **2022**, *430*, No. 132695.
(37) Dai, C. A.; Yen, W. C.; Lee, Y. H.; Ho, C. C.; Su, W. F. Facile synthesis of well-defined block copolymers containing regioregular poly(3-hexyl thiophene) via anionic macroinitiation method and their self-assembly behavior. *J. Am. Chem. Soc.* **2007**, *129* (36), 11036−11038.
(38) Lim, H.; Huang, K. T.; Su, W. F.; Chao, C. Y. Facile Syntheses, Morphologies, and Optical Absorptions of P3HT Coil-Rod-Coil Triblock Copolymers. *J. Polym. Sci., Part A:Polym. Chem.* **2010**, *48* (15), 3311−3322.
(39) Nguyen, H. Q.; Bhatt, M. P.; Rainbolt, E. A.; Stefan, M. C. Synthesis and characterization of a polyisoprene-*b*-polystyrene-*b*-poly(3-hexylthiophene) triblock copolymer. *Polym. Chem.* **2013**, *4* (3), 462−465.
(40) Inagaki, S.; Higashihara, T. Synthesis of an ABC triblock copolymer by a bilateral Click reaction using α,ω-bifunctionalized poly(3-hexylthiophene) as an inner segment. *Polym. Chem.* **2022**, *13* (24), 3613−3618.
(41) Yu, Z. P.; Liu, N.; Yang, L.; Jiang, Z. Q.; Wu, Z. Q. One-Pot Synthesis, Stimuli Responsiveness, and White-Light Emissions of Sequence-Defined ABC Triblock Copolymers Containing Polythio-

https://doi.org/10.1021/acs.macromol.5c01262
Macromolecules 2025, 58, 8670−8685

phene, Polyallene, and Poly(phenyl isocyanide) Blocks. *Macromolecules* **2017**, *50* (8), 3204−3214.
(42) Yokoyama, A.; Miyakoshi, R.; Yokozawa, T. Chain-growth polymerization for poly(3-hexylthiophene) with a defined molecular weight and a low polydispersity. *Macromolecules* **2004**, *37* (4), 1169−1171.
(43) Jeffries-El, M.; Sauvé, G.; McCullough, R. D. Facile synthesis of end-functionalized regioregular poly(3-alkylthiophene)s via modified Grignard metathesis reaction. *Macromolecules* **2005**, *38* (25), 10346−10352.
(44) Lim, H.; Chao, C. Y.; Su, W. F. Modulating Crystallinity of Poly(3-hexylthiophene) via Microphase Separation of Poly(3-hexylthiophene)-Polyisoprene Block Copolymers. *Macromolecules* **2015**, *48* (10), 3269−3281.
(45) Rahimi, K.; Botiz, I.; Agumba, J. O.; Motamen, S.; Stingelin, N.; Reiter, G. Light absorption of poly(3-hexylthiophene) single crystals. *RSC Adv.* **2014**, *4* (22), 11121−11123.
(46) Böckmann, M.; Schemme, T.; de Jong, D. H.; Denz, C.; Heuer, A.; Doltsinis, N. L. Structure of P3HT crystals, thin films, and solutions by UV/Vis spectral analysis. *Phys. Chem. Chem. Phys.* **2015**, *17* (43), 28616−28625.
(47) Willcock, H.; Lu, A.; Hansell, C. F.; Chapman, E.; Collins, I. R.; O'Reilly, R. K. One-pot synthesis of responsive sulfobetaine nanoparticles by RAFT polymerisation: the effect of branching on the UCST cloud point. *Polym. Chem.* **2014**, *5* (3), 1023−1030.
(48) Ethier, J. G.; Casukhela, R. K.; Latimer, J. J.; Jacobsen, M. D.; Shantz, A. B.; Vaia, R. A. Deep Learning of Binary Solution Phase Behavior of Polystyrene. *ACS Macro Lett.* **2021**, *10* (6), 749−754.
(49) Qian, J.; Lu, Y.; Chia, A.; Zhang, M.; Rupar, P. A.; Gunari, N.; Walker, G. C.; Cambridge, G.; He, F.; Guerin, G.; et al. Self-Seeding in One Dimension: A Route to Uniform Fiber-like Nanostructures from Block Copolymers with a Crystallizable Core-Forming Block. *ACS Nano* **2013**, *7* (5), 3754−3766.
(50) Roesing, M.; Howell, J.; Boucher, D. Solubility Characteristics of Poly(3-hexylthiophene). *J. Polym. Sci., Part B:Polym. Phys.* **2017**, *55* (14), 1075−1087.
(51) Wright, D. B.; Patterson, J. P.; Gianneschi, N. C.; Chassenieux, C.; Colombani, O.; O'Reilly, R. K. Blending block copolymer micelles in solution; obstacles of blending. *Polym. Chem.* **2016**, *7* (8), 1577−1583.
(52) Zhu, J.; Zhang, S.; Zhang, K.; Wang, X.; Mays, J. W.; Wooley, K. L.; Pochan, D. J. Disk-cylinder and disk-sphere nanoparticles via a block copolymer blend solution construction. *Nat. Commun.* **2013**, *4*, 3297.
(53) Lu, Y.; Gao, J.; Ren, Y.; Ding, Y.; Jia, L. Synergetic Self-Assembly of Liquid Crystalline Block Copolymer with Amphiphiles for Fabrication of Hierarchical Assemblies. *Small* **2024**, *20* (1), 2304955.
(54) Jiang, J. J.; Nikbin, E.; Plaha, T. S.; Howe, J. Y.; Winnik, M. A. Crystallization-Driven Self-Assembly of Polyferrocenyldimethylsilane Block Copolymers with the Corona Modified with Pendant Amino Groups. *Macromolecules* **2024**, *57* (7), 3109−3120.
(55) Jeong, G.; Choi, S.; Jang, M.; Chang, M. Thermal annealing effects on the morphology and charge transport of polymer semiconductor nanowires aligned in an insulating polymer matrix. *Dyes Pigm.* **2021**, *185*, No. 108962.
(56) Wolf, C. M.; Guio, L.; Scheiwiller, S. C.; O'Hara, R. P.; Luscombe, C. K.; Pozzo, L. D. Blend Morphology in Polythiophene-Polystyrene Composites from Neutron and X-ray Scattering. *Macromolecules* **2021**, *54* (6), 2960−2978.

https://doi.org/10.1021/acs.macromol.5c01262
Macromolecules 2025, 58, 8670−8685